

11 **Abstract**

12 We present results from the Community Climate System Model 3 (CCSM3) forced
13 with early to middle Miocene (~20 – 14 Ma) vegetation, topography, bathymetry and modern
14 CO₂. A decrease in the meridional temperature gradient of 6.5°C and an increase in global
15 mean temperature of 1.5°C are modelled in comparison with a control simulation forced with
16 modern boundary conditions. Seasonal poleward displacements of the subtropical jet streams
17 and storm tracks compared to the control simulation are associated with changes in Hadley
18 circulation and significant cooling of the polar stratosphere, consistent with previously
19 predicted effects of global warming. Energy budget calculations indicate that reduced albedo
20 and topography were responsible for Miocene warmth in the high latitude northern
21 hemisphere while a combination of increased ocean heat transport and reduced albedo was
22 responsible for relative warmth in the high latitude southern hemisphere, compared to the
23 present. Our model-data analysis suggests Miocene climate was significantly warmer and
24 wetter than shown in our simulation, consistent with previous uncoupled Miocene models
25 and supports recent reconstructions of Miocene CO₂ substantially higher than present.

26

27 Keywords: Miocene, atmosphere, climate, CCSM3.

28 **1. Introduction**

29 Relative warmth during the early to middle Miocene is well documented in marine
30 and terrestrial records. Benthic oxygen isotope data depict a peak in deep water temperatures
31 at 17 – 14.5 Ma (Zachos et al. 2008) termed the Miocene climatic optimum, after which a
32 significant positive isotopic shift is associated with growth of the Antarctic ice-sheet and a
33 drop in deep water and high latitude sea-surface temperatures (SSTs). During the Miocene
34 climatic optimum deep waters were approximately 5 - 6°C warmer than present (Lear et al.
35 2000; Zachos et al. 2008), tropical vegetation extended poleward (Cosgrove et al. 2002;
36 Wolfe 1985) and the East-Antarctic ice-sheet was smaller than present (Pekar and DeConto
37 2006).

38 Although records of Miocene warming are clear, the mechanisms responsible are not.
39 The role of CO₂ is controversial, with Alkenone- and Boron-based proxies suggesting
40 concentrations similar to or lower than present (Pagani et al. 1999; Pearson and Palmer 2000)
41 and leaf stomata indicators suggesting concentrations significantly higher (Kürschner et al.
42 2008). Changes in ocean gateways and bathymetry have also long been proposed as catalysts
43 for warming via modifications to ocean heat transport (Flower and Kennett 1994; Lagabriele
44 et al. 2009; Poore et al. 2006; Ramsay et al. 1998; Schnitker 1980; Woodruff and Savin
45 1989). However, analysis of some of the concomitant tectonic events (Wright and Miller
46 1996), the proposed mechanisms involved in gateway-induced warming (Sloan et al. 1995)
47 and more recently coupled atmosphere-ocean modelling (Huber and Sloan 2001) show that
48 such changes are not an easy explanation for global warmth. Nonetheless, numerous
49 independent tectonic events occurred during the Miocene and the lack of a ‘smoking gun’ for
50 the observed climate change implies a causal and cumulative relationship (Potter and
51 Szatmari 2009), though no hypothesis satisfactorily explains a connection. Furthermore,
52 sparse spatial and temporal coverage of climate proxies has limited the characterisation of

53 global Miocene climate (Fig. 1a), although a renewed interest in Neogene environments has
54 greatly improved coverage in some regions (NECLIME, <http://www.neclime.de/>).

55 Various numerical models have been used to explore Miocene climate, including
56 sensitivity to CO₂ (Micheels et al. 2009a; Steppuhn et al. 2007; Tong et al. 2009; You et al.
57 2009), SSTs (Herold et al. 2010; Lunt et al. 2008c; Steppuhn et al. 2006), vegetation (Dutton
58 and Barron 1997; Micheels et al. 2009b; Micheels et al. 2007), bathymetry (Barron and
59 Peterson 1991; Bice et al. 2000; Butzin et al. 2011; von der Heydt and Dijkstra 2006) or some
60 combination of these (Fluteau et al. 1999; Henrot et al. 2010; Herold et al. 2011; Kutzbach
61 and Behling 2004; Langebroek et al. 2009; Micheels et al. In Press; Ruddiman et al. 1997).
62 However, due to the relatively recent advent of coupled atmosphere-ocean models for deep
63 time paleoclimate analysis the majority of above studies have relied on prescribing SSTs or
64 ocean heat fluxes. Consequently such studies are significantly limited by uncertainties in the
65 paleoclimate record or by the simplifying assumptions of ocean heat transport. In a recent
66 study utilising a coupled atmosphere-ocean model, von der Heydt and Dijkstra (2006) use
67 version 1.4 of the Community Climate System Model (CCSM) to analyse the reversal of
68 Panama throughflow between the Oligocene and early Miocene. They link this reversal to
69 changing dimensions of Southern Ocean gateways and closing of the Tethys gateway. Using
70 the Community Earth System Models (COSMOS), Micheels et al. (In Press) take advantage
71 of the data-independence of the coupled modelling framework to analyse heat transport
72 during the late Miocene. They find a decrease in northern hemisphere ocean heat transport
73 compared to the present, likely due to the open Panama gateway in the late Miocene, and a
74 compensating increase in atmospheric heat transport. In this study we present results from
75 version 3 of the CCSM forced with global Miocene boundary conditions to investigate their
76 effect on atmosphere and land climate. An important advance in our study is the
77 representation of Miocene vegetation, topography and bathymetry (c.f. von der Heydt and

78 Dijkstra 2006). In a companion study we focus on the ocean circulation results (Herold, N.,
79 M. Huber, R.D. Müller and M. Seton, in revision, *Paleoceanography*). While the nonlinearity
80 of Miocene warming (e.g. Miller et al. 1991) suggests complex feedbacks between multiple
81 processes were involved (Holbourn et al. 2005; Shevenell et al. 2008) and uncertainty
82 remains with respect to the causes of Miocene warmth, this study focuses on the mean
83 background climate of the early to middle Miocene.

84

85 **2. Model description**

86 The CCSM3 consists of four component models of the atmosphere, ocean, land and
87 sea-ice (Collins et al. 2006). Each model operates at an independent time step and
88 communicates via a coupler. The atmosphere is represented with a hybrid sigma-pressure
89 coordinate system resolving 26 vertical levels. The land model resolves 10 soil layers, up to
90 five snow layers and 16 plant functional types. Each land grid cell consists of up to four plant
91 functional types. Both the land and atmosphere models share a horizontal T31 spectral grid,
92 representing a resolution of $3.75^\circ \times \sim 3.75^\circ$ in longitude and latitude, respectively. The ocean
93 and sea-ice models operate on a horizontal stretched grid of approximately $3^\circ \times \sim 1.5^\circ$ in
94 longitude and latitude, respectively, with coarser resolution at middle latitudes and finer
95 resolution at the poles and equator.

96 The CCSM3 has been utilised extensively for present and future climate simulations
97 (Meehl et al. 2007) as well as for simulations of the late Permian (Kiehl and Shields 2005)
98 and Eocene epochs (Shellito et al. 2009). The low resolution CCSM3, which corresponds
99 closely to the resolution chosen in this study, allows for quick equilibration of multi-century
100 simulations while maintaining a robust steady state climate (Yeager et al. 2006). However,
101 Yeager et al. (2006) note excessive sea-ice production in both hemispheres under modern
102 boundary conditions in this configuration of the CCSM3. Ocean heat transport is also

103 underestimated and southern hemisphere storm tracks displaced equatorward compared to
104 observations. Conversely, volume transport by the Antarctic Circumpolar Current is closer to
105 observed values and eastern boundary current SST biases are least severe in the low
106 resolution CCSM3, compared with higher resolution configurations (Yeager et al. 2006).

107

108 **3. Experiment design**

109 Our Miocene case is configured with topography and bathymetry from Herold et al.
110 (2008), with minor adjustments to sea level and the Tethys gateway (c.f. Fig. 1a). Dating of
111 Tethys gateway closure(s) is controversial with most evidence suggesting terminal closure by
112 the middle Miocene (Ramsay et al. 1998; Rögl 1999). As some researchers have attributed
113 early to middle Miocene warmth to Tethyan outflow of relatively warm, saline deep water
114 (Flower and Kennett 1995; Ramsay et al. 1998; Woodruff and Savin 1989) we choose an
115 open configuration to enable such outflow to occur. Major topographic differences between
116 the Miocene and modern day are accounted for by paleo-elevation estimates and include
117 areas such as the Tibetan Plateau and Andean Cordillera (see Herold et al. (2008) for details).
118 Plant functional types are prescribed based on Herold et al. (2010).

119 Concentrations of CO₂ during the Miocene are controversial. In this study we
120 prescribe a concentration of 355 ppmv, midway between the majority of Miocene estimates
121 and the same as used in 1990 control CCSM3 experiments. N₂O and CH₄ are set to pre-
122 industrial concentrations of 270 ppb and 760 ppb, respectively. Aerosol radiative forcing is
123 significantly reduced from the modern. The solar constant is set to 1365 W/m² (compared to
124 1367 W/m² for control CCSM3 simulations) and obliquity, eccentricity and precession are set
125 to values appropriate for 1950.

126 Initial ocean temperatures and salinities are based on modern global depth averages.
127 This arbitrary initialisation results in an ocean equilibration time of approximately 800 years,

128 which is evaluated based on depth-integrated ocean mean temperature. We integrate the
129 model for a further 300 years and use the mean of the last 100 years for analysis. Residual
130 energy flux at the surface and top of the model for the final 100 years is 0.1 W/m^2 and
131 volume mean ocean temperature drift is $< 0.01^\circ\text{C}$ per century (Table 1). We compare our
132 Miocene case with a control case forced with modern boundary conditions appropriate for
133 1990, including a CO_2 concentration of 355 ppmv.

134

135 **4. Results**

136 *a. Surface temperature*

137 Global annual surface temperature is 1.5°C higher in the Miocene compared to the
138 control case (Table 1). Zonal mean tropical temperatures in the Miocene are 0.5°C lower
139 while polar temperatures are approximately 6°C higher, resulting in a 6.5°C lowering of the
140 meridional temperature gradient (Fig. 2a). Maximum warming at both poles in the Miocene
141 relative to the control case is approximately equal, however, the majority of polar warming in
142 the northern hemisphere manifests over land, in contrast to the meagre temperature increase
143 over Antarctica (Fig. 2b). At low to middle latitudes, patterns of mean annual surface
144 temperature do not vary considerably between the Miocene and control cases, with most
145 isotherms shifted poleward by several degrees in the Miocene (Fig. 3c and f). Parts of
146 Australia are more than 3°C cooler in the Miocene as it lay outside of the tropics. Reduced
147 Miocene topography in Greenland and North America contributes to higher annual
148 temperatures in these regions. Summertime temperatures in Greenland and a large portion of
149 the Arctic Ocean are above freezing in the Miocene, in contrast to the control case (Fig. 3a
150 and d). A significant portion of the modelled surface warming, particularly at high latitudes,
151 can be attributed to the prescribed darker and broader leaved Miocene vegetation compared
152 to the control case (Herold et al. 2010). Dutton and Barron (1997) showed that differences in

153 vegetation between the present and Miocene contribute a 1.9°C global warming effect.
154 Similarly, Otto-Bliesner and Upchurch (1997) showed that a vegetated versus un-vegetated
155 Cretaceous world results in a 2.2°C global warming. More recent studies with less idealised
156 vegetation distributions show the same sign of sensitivity to vegetation, though of a
157 significantly smaller magnitude. Micheels et al. (2007) report a climate sensitivity to late
158 Miocene vegetation of 0.9°C, while Henrot et al. (2010) report a 0.5°C sensitivity to middle
159 Miocene vegetation, relative to modern vegetation. Given that total global warming in our
160 Miocene case is 1.5°C relative to the control case, in lieu of a sensitivity experiment we
161 speculate that the warming from our Miocene vegetation alone is closer to these latter studies.
162 Significant increases in continental seasonality occur in the Miocene northern hemisphere
163 due namely to the greater surface area of Eurasia and North America (Fig. 3d and e).

164

165 *b. Atmospheric temperature*

166 Miocene temperatures in the polar troposphere and stratosphere (above 200 mb) are
167 warmer and cooler than the control case respectively, particularly in the northern hemisphere,
168 resulting in a larger vertical temperature gradient (Fig. 4c and d). Cooling of the northern
169 polar stratosphere during wintertime increases relative humidity and consequently increases
170 high altitude cloud fraction by up to 20% (not shown). However, a corresponding southern
171 hemisphere wintertime cooling is not observed (Fig. 4c). Substantially greater summertime
172 warming occurs in the northern polar troposphere compared to the southern polar troposphere
173 in the Miocene (c.f. Fig. 4c and d). This is associated with the large increase in surface area
174 of northwest Eurasia as well as reduced surface albedo across northeast North America and
175 Greenland. Comparatively little albedo change – and thus temperature change – is modelled
176 over the Antarctic continent during the southern hemisphere summer. Interestingly, the
177 majority of warming which occurs in the southern polar troposphere occurs concomitantly

178 with warming in the northern polar troposphere, though to a lesser degree (Fig. 4c). This is
179 attributed to the greatest decrease in Southern Ocean sea-ice occurring during southern
180 hemisphere wintertime, driven by significant Weddell Sea bottom water formation (Herold,
181 N., M. Huber, R.D. Müller and M. Seton, in revision, *Paleoceanography*).

182

183 *c. Jet streams and storm tracks*

184 The subtropical jet streams in the Miocene are weaker than our control case (Fig. 5),
185 an expected result given the lower meridional temperature gradient (Fig. 2a). The subtropical
186 jet streams are displaced poleward and slightly upward during December-January-February
187 (DJF), though not during June-July-August (JJA; Fig. 5c and d). Similarly, intensification of
188 the Miocene northern polar jet stream occurs during DJF, though no corresponding
189 intensification of the southern hemisphere polar jet stream is observed during JJA, mirroring
190 simulated stratospheric temperature changes (previous section). Consistent with zonal
191 circulation changes, the zonal distribution of eddy kinetic energy indicates a poleward
192 displacement of middle latitude storms during DJF in both hemispheres, though only a
193 weakening of storm tracks during JJA (Fig. 6). The poleward displacement of eddy kinetic
194 energy is also consistent with a poleward shift in Hadley circulation (Fig. 7).

195

196 *d. Seasonal precipitation and surface winds*

197 The Miocene case exhibits broad increases in mean annual precipitation over central
198 and northern Africa, northern Eurasia and North America ($>50^{\circ}\text{N}$) and Greenland, the
199 majority of which falls during JJA (Fig. 8a and d). Due to the variation in plate configurations
200 between the Miocene and present day, anomaly plots between the two cases are ineffective at
201 examining the regional monsoons. Therefore we examine DJF minus JJA surface wind and
202 precipitation fields for each case, which enables a qualitative assessment of monsoon strength

203 and seasonal drying/wetting (Fig. 8 and 9). In the Miocene case smaller seasonal variations in
204 wind strength relative to the control case are modelled over India, the Arabian Sea, the South
205 China Sea and along the coast of the northwest Pacific Ocean (Fig. 9c and f). These
206 differences reflect a weakening of JJA onshore winds from the Arabian Sea and weakening of
207 DJF offshore winds in the northwest Pacific Ocean in the Miocene. In contrast, stronger JJA
208 onshore winds over the Bay of Bengal occur in the Miocene case. These changes are
209 accompanied by greater maxima in seasonal precipitation change over southern and eastern
210 Eurasia in the Miocene relative to the control case (Fig. 8c and f). In each instance this is due
211 overwhelmingly to higher JJA precipitation in the Miocene case than to differences in DJF
212 precipitation (Fig. 8a and d). More northward landfall of summer precipitation into northeast
213 China in the Miocene case (Fig. 8a and d) is consistent with luvisols indicating greater
214 northward moisture transport compared to the Quaternary (Guo et al. 2008). Generally,
215 however, the changes in Asian monsoon strength between our Miocene and control cases are
216 not strong relative to the simulated effects of Tibetan Plateau uplift or Paratethys expansion
217 (Zhongshi et al. 2007a). As the Tibetan Plateau has a near modern elevation in our Miocene
218 case, such effects are minimal (Fig. 1).

219 The present day asymmetry in seasonality about the Rocky Mountains is amplified in
220 the Miocene case, with wetter winters to the northwest and wetter summers to the southeast
221 (Fig. 8c and f). This is in contrast to paleobotanical evidence suggesting wet summers in the
222 western United States (Lyle et al. 2008). Summertime onshore winds over northern Australia
223 are substantially weaker in the Miocene case and thus summer monsoon precipitation is
224 significantly weaker over the northern half of the continent. We do not relate this to reduced
225 atmospheric outflow from the Asian winter monsoon (see Miller et al. 2005) but to the
226 location of Australia within the subtropical high in the Miocene. Relatively modest
227 sensitivities to changes in local and global boundary conditions demonstrates the robustness

228 of a weaker Australian monsoon in our model (Herold et al. 2011). In northern Africa,
229 summer precipitation is significantly higher in the Miocene due to the replacement of desert
230 with broadleaf vegetation (Fig. 8a and d), consistent with the sensitivity study of Micheels et
231 al. (2009b).

232

233 *e. Energy budget*

234 Atmospheric heat transport differs little between the Miocene and control cases with
235 the largest difference being a weaker peak at 45°N in the Miocene by 0.5 PW (Fig. 10).
236 Similarly, ocean heat transport decreases in the northern hemisphere by approximately the
237 same magnitude, thus changes in atmospheric heat transport do not compensate for changes
238 in ocean heat transport (or vice versa) as modelled by Micheels et al. (In Press). Decreased
239 northern hemisphere ocean heat transport in the Miocene case is a result of a significant
240 weakening of North Atlantic Deep Water formation (see Herold, N., M. Huber, R.D. Müller
241 and M. Seton, in revision, *Paleoceanography* for details). A slight poleward shift in peak
242 atmospheric heat transport is associated with a poleward shift in peak eddy kinetic energy
243 (Fig. 6). A near-zero residual surface energy flux at latitudes greater than 60°N indicates
244 radiative equilibrium is achieved without a compensating ocean heat transport (Fig. 11). This
245 increase in residual surface energy compared to the control case is due primarily to greater
246 incoming net surface energy over the sub-Arctic continents in association with vegetation and
247 topography changes. Southern hemisphere heat transport by the atmosphere decreases
248 slightly, though is over compensated by an increase in ocean heat transport.

249

250 *f. Quantitative comparison with climate proxies*

251 While proxy records are inconsistently distributed (Fig. 1a) and often subject to large
252 uncertainties (as discussed by Herold et al. 2010), they provide the only means of ground

253 truth for our Miocene case. Comparisons between models and proxies also introduce their
254 own bias due to inherent model uncertainties. The CCSM3 is capable of stable multi
255 millennial climate simulations and is significantly improved over earlier versions. However,
256 it contains significant systematic biases in modelling the present climate (Collins et al. 2006).
257 For example, the high resolution CCSM3 simulates mean summer 2 meter air temperatures
258 up to $\pm 16^{\circ}\text{C}$ different from observations (Collins et al. 2006). Somewhat surprisingly, the
259 same discrepancy is smaller for our low resolution control case, though of a similar
260 magnitude. Thus we compare the differences in 2 meter air temperature and precipitation
261 between our Miocene and control cases to the differences between Miocene proxy records
262 and modern observations (Tables 2 and 3). 2 meter air temperature is chosen as it is a closer
263 representation of the forest canopy, from which most terrestrial proxies of climate are
264 derived. Examination of table 2 clearly shows that simulated changes in temperature at proxy
265 localities (the ‘Simulated warming’ column) are significantly lower than the changes based
266 on modern observations and proxy records (the ‘Proxy derived warming’ column). The mean
267 warming across all proxy locations between our Miocene and control cases is 1.3°C ,
268 compared to 5.9°C between observations and proxies (Table 2). Thus our Miocene case is
269 significantly too cool. The largest differences between simulated and observed Miocene
270 warmings occur at middle to high latitude localities, indicating that the meridional
271 temperature gradient is significantly steeper than indicated by proxies, consistent with
272 previous Miocene climate modelling (Steppuhn et al. 2007; Tong et al. 2009).

273 We note that there is a clear distribution bias toward the Tethys Sea (Fig. 1a), thus
274 model-data discrepancies are not necessarily indicative of global model performance.
275 However, the mean simulated warming amongst proxy sites (1.3°C ; Table 2) is similar to the
276 mean global warming between the Miocene and control cases (1.5°C ; Table 1). Precipitation
277 change follows a similar trend to 2 meter air temperature, with differences between

278 observations and proxies significantly higher than the differences between our Miocene and
279 control cases (Table 3).

280

281 **5. Discussion**

282 *a. Miocene warmth*

283 Our Miocene case exhibits a decrease in the meridional temperature gradient of 6.5°C
284 and an increase in global mean temperature of 1.5°C compared with our control case, without
285 a higher CO₂. This warming is equivalent to the transient climate response of the CCSM3 to a
286 doubling of CO₂ (Kiehl et al. 2006) and suggests that differences in topography, bathymetry
287 and vegetation contributed significantly to Miocene warmth. However, the middle latitude
288 divergence of modelled temperature change from observed temperature change indicates that
289 the Miocene case's meridional temperature gradient is too steep (Table 2) and that global
290 mean temperature was higher than simulated here. This is consistent with previous Miocene
291 studies using slab (Micheels et al. 2007; Steppuhn et al. 2007; Tong et al. 2009; You et al.
292 2009) and dynamical ocean models (Micheels et al. In Press).

293 High latitude warming in our Miocene case is compensated to a large extent by
294 meagre increases and even decreases in tropical temperatures (Fig. 3f). This is in stark
295 contrast to the late Miocene coupled atmosphere-ocean simulation by Micheels et al. (In
296 Press), which exhibits zonal mean tropical temperatures over 1°C warmer than modern (their
297 Fig. 3a). A large portion of this difference can be attributed to increased upwelling of cool
298 waters in the tropical Pacific in our Miocene case, ostensibly as a response to the open
299 Panama gateway. A similar surface temperature response to opening of the Panama gateway
300 is simulated by Lunt et al. (2008a). The reconciliation of simulated tropical temperatures with
301 proxy records is precluded by the absence or poor fidelity of data.

302 Northern hemisphere polar stratospheric cooling in the Miocene case occurs almost
303 entirely during polar night, decreasing minimum temperatures to approximately -88.8°C (Fig.
304 4d). This is several degrees below the formation threshold of stratospheric clouds ($\sim -83.2^{\circ}\text{C}$),
305 suggesting these may have been a viable mechanism for high latitude warming (e.g. Sloan
306 and Pollard 1998). We note that the region of stratospheric temperatures below the formation
307 threshold in our Miocene case is small ($>80^{\circ}\text{N}$) and that lower temperatures would likely be
308 required before stratospheric clouds could have a significant surface effect (Rosenfield 1993).
309 However, higher concentrations of stratospheric CH_4 (Beerling et al. 2009) and a warmer
310 tropical tropopause (Randel et al. 2006) due to higher CO_2 (e.g. Kürschner et al. 2008) may
311 have further promoted conditions conducive to stratospheric cloud formation.

312 Due to sparse and ambiguous proxy records the timing of northern hemisphere
313 glaciation has been the subject of debate. Sediment records from the central Arctic basin
314 indicate the existence of sea-ice from ~ 45 Ma (Moran et al. 2006) and ice-rafted-debris
315 indicate isolated glaciers in Greenland between 30 – 38 Ma (Eldrett et al. 2007), much earlier
316 than previous records suggested (e.g. Larsen 1994; Zachos et al. 2001). However, the onset of
317 major permanent ice-sheets in Greenland likely did not occur until CO_2 dropped below pre-
318 industrial concentrations (DeConto et al. 2008; Lunt et al. 2008b). This latter supposition is
319 supported here by simulated above-freezing summertime temperatures over Greenland in our
320 Miocene case (Fig. 3a and d), despite a modern CO_2 and an overproduction of sea-ice
321 (Herold, N., M. Huber, R.D. Müller and M. Seton, in revision, *Paleoceanography*). This
322 surface warming compared to our control case is attributable to the lower elevation and
323 prescribed needleleaf vegetation of Greenland in the Miocene case.

324 Miocene heat transport by the atmosphere is lower in the northern hemisphere and
325 consequently does not contribute to the higher surface temperatures relative to the control
326 case (Fig. 10). The near-zero residual surface energy flux at latitudes greater than 60°N (Fig.

327 11) indicates that the net effect of ocean heat transport is also negligible in the Miocene, as
328 shown by a more than halving of ocean heat transport past this latitude (Fig. 10).
329 Consequently, changes in albedo and topography are responsible for high latitude northern
330 hemisphere warming. This is consistent with models of early (Heinemann et al. 2009) and
331 late (Haywood and Valdes 2004) Cenozoic climates as well as various sensitivity studies
332 (Dutton and Barron 1997; Otto-Bliesner and Upchurch 1997). Conversely, Miocene high
333 southern latitudes show near identical atmospheric heat transport compared to the control
334 case though a slightly lower residual surface energy flux (Fig. 11) and greater ocean heat
335 transport (Fig. 10; Herold, N., M. Huber, R.D. Müller and M. Seton, in revision,
336 *Paleoceanography*), resulting in significantly higher surface temperatures over the ocean (c.f.
337 Fig. 2a and 2b). This high latitude warming occurs predominantly at the site of Weddell Sea
338 bottom water formation and to a lesser extent at gird points converted from land in the control
339 case to ocean in the Miocene case (Fig. 3f). Thus the majority of high latitude southern
340 hemisphere warming is due to heat transport to the Weddell Sea and albedo changes
341 associated with a smaller Antarctic continent.

342

343 *b. Seasonal hydrology*

344 Recent sensitivity studies have demonstrated that in addition to Tibetan Plateau uplift
345 (Prell and Kutzbach 1992), shrinking of the Lago-Mare (Zhongshi et al. 2007a) and
346 expansion of the South China Sea (Zhongshi et al. 2007b) were critical to the development of
347 a monsoon climate in Asia. Our results support the transition to a modern monsoon climate
348 by the early Miocene, as indicated by an exhaustive analysis of proxy records from the
349 Paleocene to present (Guo et al. 2008). While uncertainty exists regarding the area and
350 elevation of the Miocene Tibetan Plateau (Harris 2006 and references therein; Wang et al.
351 2008), the precipitation patterns shown here would likely be robust under a wide range of

352 imposed elevations (Prell and Kutzbach 1992; Zhongshi et al. 2007a). Furthermore, model
353 simulations have demonstrated that the size of the Lago-Mare has little impact on the
354 development of the East Asian monsoon once the elevation of the Tibetan Plateau reaches
355 approximately 3,000 m, and thus is not a large source of uncertainty in our study (Zhongshi et
356 al. 2007a; Zhongshi et al. 2007b). Expectedly then, the existence and dimensions of the Asian
357 monsoon in our Miocene case has been largely predetermined by the near-modern elevation
358 of the Tibetan Plateau.

359 The northwest coast of the United States experiences higher wintertime precipitation
360 in the Miocene case, though no change in summertime precipitation (Fig 8). Additionally, no
361 change in summertime effective moisture (evaporation minus precipitation) is observed (not
362 shown). This reflects an amplification of modern day seasonality when conversely fossil flora
363 indicate wet summers along the west coast during the Miocene (Lyle et al. 2008). It has been
364 suggested that wetter summers in the western United States may have been driven by warmer
365 North Pacific SSTs (Lyle et al. 2003). The warmer SSTs in our Miocene case suggest that
366 this was not the case. Unpublished results from an identical Miocene simulation run with a
367 CO₂ concentration of 560 ppmv shows greater annual precipitation along the west coast of
368 Canada but no significant change in the western United States. Alternatively, Ruddiman and
369 Kutzbach (1989) find that relatively high North American topography results in summer
370 drying of the west coast due to onshore winds acquiring a more northerly aspect. This is
371 associated with the western limb of the deepening summer low that forms over North
372 America as mountain ranges are uplifted (Ruddiman and Kutzbach 1989). Northerly winds in
373 summer are observed along the west coast in both cases (Fig. 9a and d). The uplift history of
374 North America is controversial although a recent isotope study suggests high elevations by
375 the Eocene-Oligocene (Mix et al. 2011), which is broadly reflected by the prescribed
376 elevation in our model (75% of the modern; Herold et al. 2008). Thus, if lower elevations are

377 considered then this may partially explain the absence of wet summers along the west coast
378 in our Miocene case. We also note that reproduction of precipitation patterns are significantly
379 improved under the high resolution configurations of the CCSM3 (c.f. Meehl et al. 2006) and
380 improved convection schemes (Boos and Kuang 2010).

381

382 *c. Atmospheric changes*

383 The poleward shift of the subtropical jet streams in the Miocene is consistent with
384 model simulations of increasing CO₂ (Lorenz and DeWeaver 2007). However, the entire shift
385 in our Miocene case occurs during DJF (Fig. 5). The timing and seasonal nature of these
386 changes may be attributable to the sensitivity of the subtropical jet streams to extratropical
387 stratospheric cooling (Polvani and Kushner 2002; Fig. 4). Polvani and Kushner (2002) show
388 that cooling of the polar stratosphere causes a poleward shift of the subtropical jet stream, a
389 response which strengthens with increases in lapse rate. Thus as no significant cooling of the
390 northern hemisphere polar stratosphere occurs during JJA (c.f. Fig. 4c and d), no poleward
391 shift of the summer subtropical jet streams is simulated (Fig. 5c). The significant increase in
392 the northern hemisphere polar vertical temperature gradient during DJF (Fig. 4d) is also
393 responsible for the stronger zonal wind response of the northern polar jet compared to the
394 southern hemisphere (Fig. 5d). This stronger cooling increases relative humidity which
395 subsequently fuels cloud genesis. However, the cause of this cooling, and why it occurs only
396 in the northern hemisphere during winter, is not clear from model diagnostics. Interestingly,
397 uniform bipolar cooling of the stratosphere is modelled in modern doubled CO₂ experiments
398 (Rind et al. 1998) and under Paleocene boundary conditions (Rind et al. 2001), suggesting the
399 uni-polar response in our results may be a consequence of Miocene topography.

400 Miocene eddy kinetic energy maxima also shift poleward during DJF (Fig. 6d).
401 However, only the northern hemisphere storm tracks intensify during these months, while the

402 southern hemisphere storm tracks weaken. During JJA, both northern and southern
403 hemisphere storm tracks weaken in the Miocene (Fig. 6c). Poleward shift of the storm tracks,
404 like zonal circulation, is consistent with the effects of increasing CO₂ (Yin 2005). Similarly,
405 the modelled expansion of the Hadley cells are consistent with an increase in global mean
406 temperature (Frierson et al. 2007).

407

408 *d. Experiment caveats*

409 Biases in the low resolution CCSM3 have been previously documented and relate
410 chiefly to coarse resolution, component coupling and parameterisation of sub grid scale
411 processes (Stan et al. 2010; Yeager et al. 2006). Modelling time periods prior to instrument
412 records adds further uncertainty regarding model boundary conditions. Parameter biases may
413 also be more or less severe in paleoclimate simulations (e.g. Lyle 1997).

414 Uncertainties in our topography and bathymetry exist due to 1) the low resolution
415 with which the CCSM3 represents the physical Earth. The ramifications of low model
416 resolution on model-data comparisons is problematic, as discussed in Herold et al. (2010). 2)
417 Availability of geological evidence limiting our ability to constrain tectonic events in high
418 temporal and spatial detail. For example, fossil flora and oxygen isotope paleoaltimetry
419 suggests that the southern and central Tibetan Plateau reached near modern elevations by 15
420 Ma (Spicer et al. 2003) or even 35 Ma (Rowley and Currie 2006), however, relatively little is
421 known of the corresponding lateral and north-south uplift of the plateau (Harris 2006 and
422 references therein). Thus the near modern elevation of the entire Tibetan Plateau in our
423 topography may represent the upper end of possibilities.

424 Miocene bathymetry is also subject to large uncertainties in areas such as the North
425 Atlantic and Drake Passage. At present, the Greenland-Scotland-Ridge provides a crucial
426 barrier to deep water outflow from the Greenland-Norwegian Seas. However, given that no

427 deep water formation occurs in the Greenland-Norwegian Seas in our Miocene case the
428 climatic effect of changes in sill depth are uncertain. The relatively deep Greenland-Scotland-
429 Ridge in our Miocene case (Fig. 1) appears to be crucial to the northward flow of warm
430 subtropical water below the mixed-layer and it is unclear what effect the blocking of this
431 water would have on surface climate (see Herold, N., M. Huber, R.D. Müller and M. Seton,
432 in revision, *Paleoceanography*). The depth of the Drake Passage is important in determining
433 the formation of North Atlantic Deep Water. Gradual deepening of the Drake Passage has
434 been shown to initiate North Atlantic Deep Water formation, consequently warming the
435 North Atlantic and cooling the South Atlantic (Sijp and England 2004). While the timing of
436 the Drake Passage opening is controversial it is generally believed to have been at near
437 modern depths by the Miocene. However, it has been suggested that temporary constriction
438 of the passage prior to the middle Miocene may have weakened the Antarctic Circumpolar
439 Current and contributed to Miocene warming (Lagabrielle et al. 2009).

440 Miocene vegetation is reconstructed from 29 macrofossil records (Wolfe 1985) with
441 minor amendments (Herold et al. 2010). The exclusion of microfossils precludes grasslands
442 and by association the high pressure cells associated with Hadley circulation (Cosgrove et al.
443 2002), thus our prescribed vegetation may be associated with a climate warmer than is
444 justified. More complete compilations of fossil flora need to be synthesised into vegetation
445 distributions which consider the current understanding of Miocene hydrology and ocean and
446 atmosphere circulation. Vegetation models can also be utilised, ideally in concert with fossil
447 flora (e.g. Micheels et al. 2007). Middle Miocene vegetation distributions from a dynamic
448 global vegetation model forced with climate model output present a cooler and more detailed
449 global vegetation compared to this study (Henrot et al. 2010). However, while vegetation
450 models circumvent uncertainties in data extrapolation and assumptions of atmospheric and

451 oceanic circulation, they contain their own model uncertainties and are subject to climate
452 model bias (Shellito and Sloan 2006).

453 In addition to topography, bathymetry and vegetation small parameter differences
454 exist between our Miocene and control cases (CH_4 , N_2O , solar constant, aerosols and orbital
455 values). Such differences make the attribution of climate changes to specific boundary
456 conditions more problematic. However, based on radiative forcing estimates (e.g. Forster et
457 al. 2007) it is arguable that the reduction in our Miocene case of CH_4 and N_2O concentrations
458 as well as the solar constant would constitute a net Miocene cooling. While aerosol radiative
459 forcing is also lower in our Miocene case relative to the control case, this, along with the
460 negligible change in orbital parameters, is unlikely to result in a net cooling. However, this
461 can only be unequivocally determined by a sensitivity experiment and we also note that the
462 wavelengths of optimum absorption by different atmospheric agents overlap. In addition, our
463 control case should, if anything, be warmer than modern observations given that it has
464 equilibrated to the prescribed 1990 concentrations of greenhouse gases. This is in contrast to
465 observations which represent a transient response to radiative forcing up until the period
466 observed (1950 – 1999, Table 2). The net effect of these model inconsistencies is that the
467 simulated warming between our Miocene and control cases should be considered
468 conservative.

469 The role CO_2 played in early to middle Miocene warmth and subsequent cooling
470 continues to be a large hindrance to understanding Miocene climate. The use of modern CO_2
471 in our Miocene case plays a potentially large role in explaining the discrepancies with proxy
472 records (Tables 2 and 3). While marine based CO_2 proxies still place concentrations at
473 approximately present day values (Henderiks and Pagani 2008; Tripathi et al. 2009) recent
474 upward revisions based on pedogenic carbonates (Retallack 2009) and leaf stomata indices
475 (Kürschner et al. 2008; Retallack 2001) suggest CO_2 was considerably higher. Ice-sheet

476 modelling (DeConto et al. 2008; Lunt et al. 2008b) also supports a Miocene CO₂ at least as
477 high as the modern (c.f. Pagani et al. 1999). Furthermore, chemistry transport modelling
478 suggests CH₄ concentrations were above present during the Miocene (Beerling et al. 2009),
479 thus Miocene greenhouse forcing was very likely higher than prescribed in our Miocene case.
480 Nevertheless, a slab ocean model forced with output from our Miocene case and a doubled
481 CO₂ concentration of 710 ppmv (Herold et al. 2011) does not exhibit a sufficient lowering of
482 the meridional temperature gradient to explain our model-data discrepancies, consistent with
483 previous studies (Steppuhn et al. 2007; Tong et al. 2009; You et al. 2009).

484

485 **6. Conclusions**

486 We present quantitative constraints on the Miocene climate system incorporating
487 reconstructed vegetation, topography and bathymetry. A decrease in the meridional
488 temperature gradient of 6.5°C and increase in global mean temperature of 1.5°C compared to
489 our control case occurs without an increase in CO₂. Therefore a significant portion of
490 Miocene warmth can be attributed to factors other than greenhouse gases. Nevertheless,
491 similar to previous uncoupled models, our model-data analysis implicates above modern CO₂
492 or similar acting mechanisms during the Miocene, consistent with stomatal records
493 (Kürschner et al. 2008). More tropical and polar proxy records are required to reliably
494 constrain the meridional temperature gradient.

495 Energy budget and heat transport calculations indicate that increased ocean heat
496 transport and reduced albedo were responsible for above modern temperatures at high
497 southern latitudes in the Miocene (Herold, N., M. Huber, R.D. Müller and M. Seton, in
498 revision, *Paleoceanography*). Conversely, reduced atmosphere and ocean heat transport in
499 the northern hemisphere indicates that reduced albedo and topography were responsible for

500 warming at high northern latitudes. This dichotomy indicates that both changes in ocean
501 circulation and land characteristics were responsible for early to middle Miocene warmth.

502 Changes in atmospheric temperature, wind and eddy kinetic energy are surprisingly
503 consistent with model predictions of future global warming due to increasing CO₂. However,
504 significant intensification of the polar jet stream is only observed in the northern hemisphere.
505 Furthermore, poleward displacement of the subtropical jet streams occurs only during DJF.
506 This polar and seasonal asymmetry is attributed to significantly greater cooling of the polar
507 stratosphere during DJF, particularly in the northern hemisphere. Results from this study and
508 Herold et al. (in revision, *Paleoceanography*) suggest future work should address sensitivity
509 to various changes in topography and bathymetric choke points, along with elevated
510 greenhouse gas concentrations.

511

512 **7. Acknowledgements**

513 This research was undertaken on the NCI National Facility in Canberra, Australia,
514 which is supported by the Australian Commonwealth Government. In addition, parts of this
515 research were funded by NSF grants to MH, 0450221-EAR and 0902780-ATM. We thank
516 two anonymous reviewers for their constructive feedback.

517

518 **8. References**

519 Akgün, F., M. S. Kayseri, and M. S. Akkiraz, 2007: Palaeoclimatic evolution and
520 vegetational changes during the Late Oligocene-Miocene period in Western and
521 Central Anatolia (Turkey). *Palaeogeography, Palaeoclimatology, Palaeoecology*,
522 **253**, 56-90.

523 Barron, E. J., and W. H. Peterson, 1991: The Cenozoic ocean circulation based on ocean
524 General Circulation Model results. *Palaeogeography, Palaeoclimatology,*
525 *Palaeoecology*, **83**, 1-28.

526 Beerling, D., R. A. Berner, F. T. Mackenzie, M. B. Harfoot, and J. A. Pyle, 2009: Methane
527 and the CH₄ related greenhouse effect over the past 400 million years. *Am J Sci*, **309**,
528 97-113.

529 Bice, K. L., C. R. Scotese, D. Seidov, and E. J. Barron, 2000: Quantifying the role of
530 geographic change in Cenozoic ocean heat transport using uncoupled atmosphere and
531 ocean models. *Palaeogeography, Palaeoclimatology, Palaeoecology*, **161**, 295-310.

532 Bohme, M., A. A. Bruch, and A. Selmeier, 2007: The reconstruction of Early and Middle
533 Miocene climate and vegetation in Southern Germany as determined from the fossil
534 wood flora. *Palaeogeography, Palaeoclimatology, Palaeoecology*, **253**, 107-130.

535 Boos, W. R., and Z. Kuang, 2010: Dominant control of the South Asian monsoon by
536 orographic insulation versus plateau heating. *Nature*, **463**, 218-222.

537 Butzin, M., G. Lohmann, and T. Bickert, 2011: Miocene ocean circulation inferred from
538 marine carbon cycle modeling combined with benthic isotope records.
539 *Paleoceanography*, **26**, PA1203.

540 Collins, W. D., and Coauthors, 2006: The Community Climate System Model Version 3
541 (CCSM3). *Journal of Climate*, **19**, 2122-2143.

542 Cosgrove, B. A., E. J. Barron, and D. Pollard, 2002: A simple interactive vegetation model
543 coupled to the GENESIS GCM. *Global and Planetary Change*, **32**, 253-278.

544 DeConto, R. M., D. Pollard, P. A. Wilson, H. Palike, C. H. Lear, and M. Pagani, 2008:
545 Thresholds for Cenozoic bipolar glaciation. *Nature*, **455**, 652-656.

546 Dutton, J. F., and E. J. Barron, 1997: Miocene to present vegetation changes; a possible piece
547 of the Cenozoic cooling puzzle. *Geology*, **25**, 39-41.

- 548 Eldrett, J. S., I. C. Harding, P. A. Wilson, E. Butler, and A. P. Roberts, 2007: Continental ice
549 in Greenland during the Eocene and Oligocene. *Nature*, **446**, 176-179.
- 550 Erdei, B., L. Hably, M. Kazmer, T. Utescher, and A. A. Bruch, 2007: Neogene flora and
551 vegetation development of the Pannonian domain in relation to palaeoclimate and
552 palaeogeography. *Palaeogeography, Palaeoclimatology, Palaeoecology*, **253**, 131-
553 156.
- 554 Flower, B. P., and J. P. Kennett, 1994: The middle Miocene climatic transition: East
555 Antarctic ice sheet development, deep ocean circulation and global carbon cycling.
556 *Palaeogeography, Palaeoclimatology, Palaeoecology*, **108**, 537-555.
- 557 ———, 1995: Middle Miocene Deepwater Paleoceanography in the Southwest Pacific:
558 Relations with East Antarctic Ice Sheet Development. *Paleoceanography*, **10**.
- 559 Fluteau, F., G. Ramstein, and J. Besse, 1999: Simulating the evolution of the Asian and
560 African monsoons during the past 30 Myr using an atmospheric general circulation
561 model. *J. Geophys. Res.*, **104**, 11995-12018.
- 562 Forster, P., and Coauthors, 2007: Changes in Atmospheric Constituents and in Radiative
563 Forcing. *Climate Change 2007: The Physical Science Basis. Contribution of Working
564 Group I to the Fourth Assessment Report of the Intergovernmental Panel on Climate
565 Change*, S. Solomon, D. Qin, M. Manning, Z. Chen, M. Marquis, K.B. Averyt,
566 M. Tignor and H.L. Miller, Ed., Cambridge University Press.
- 567 Frierson, D. M. W., J. Lu, and G. Chen, 2007: Width of the Hadley cell in simple and
568 comprehensive general circulation models. *Geophys. Res. Lett.*, **34**, L18804.
- 569 Greenwood, D. R., 1994: Palaeobotanical evidence for Tertiary climates. *The History of
570 Australian Vegetation: Cretaceous to Recent*, R. S. Hill, Ed., Cambridge University
571 Press, 44-59.

572 Gregory-Wodzicki, K. M., W. C. McIntosh, and K. Velasquez, 1998: Climatic and tectonic
573 implications of the late Miocene Jakokkota flora, Bolivian Altiplano. *Journal of South*
574 *American Earth Sciences*, **11**, 533-560.

575 Guo, Z. T., and Coauthors, 2008: A major reorganization of Asian climate by the early
576 Miocene. *Climate of the Past*, **4**, 153-174.

577 Harris, N., 2006: The elevation history of the Tibetan Plateau and its implications for the
578 Asian monsoon. *Palaeogeography, Palaeoclimatology, Palaeoecology*, **241**, 4-15.

579 Haywood, A. M., and P. J. Valdes, 2004: Modelling Pliocene warmth: contribution of
580 atmosphere, oceans and cryosphere. *Earth and Planetary Science Letters*, **218**, 363-
581 377.

582 Heinemann, M., J. H. Jungclaus, and J. Marotzke, 2009: Warm Paleocene/Eocene climate as
583 simulated in ECHAM5/MPI-OM. *Clim. Past*, **5**, 785-802.

584 Henderiks, J., and M. Pagani, 2008: Coccolithophore cell size and the Paleogene decline in
585 atmospheric CO₂. *Earth and Planetary Science Letters*, **269**, 576-584.

586 Henrot, A. J., L. François, E. Favre, M. Butzin, M. Ouberdous, and G. Munhoven, 2010:
587 Effects of CO₂, continental distribution, topography and vegetation changes on the
588 climate at the Middle Miocene: a model study. *Clim. Past*, **6**, 675-694.

589 Herold, N., R. D. Müller, and M. Seton, 2010: Comparing early to middle Miocene terrestrial
590 climate simulations with geological data. *Geosphere*, **6**, 952-961.

591 Herold, N., M. Seton, R. D. Müller, Y. You, and M. Huber, 2008: Middle Miocene tectonic
592 boundary conditions for use in climate models. *Geochem. Geophys. Geosyst.*, **9**,
593 Q10009.

594 Herold, N., M. Huber, D. R. Greenwood, R. D. Müller, and M. Seton, 2011: Early to Middle
595 Miocene monsoon climate in Australia. *Geology*, **39**, 3-6.

596 Holbourn, A., W. Kuhnt, M. Schulz, and H. Erlenkeuser, 2005: Impacts of orbital forcing and
597 atmospheric carbon dioxide on Miocene ice-sheet expansion. *Nature*, **438**, 483-487.

598 Huber, M., and L. C. Sloan, 2001: Heat transport, deep waters, and thermal gradients:
599 Coupled simulation of an Eocene greenhouse climate. *Geophysical Research Letters*,
600 **28**, 3481-3484.

601 Ivanov, D., A. R. Ashraf, V. Mosbrugger, and E. Palamarev, 2002: Palynological evidence
602 for Miocene climate change in the Forecarpathian Basin (Central Paratethys, NW
603 Bulgaria). *Palaeogeography, Palaeoclimatology, Palaeoecology*, **178**, 19-37.

604 Kemp, E. M., 1978: Tertiary climatic evolution and vegetation history in the Southeast Indian
605 Ocean region. *Palaeogeography, Palaeoclimatology, Palaeoecology*, **24**, 169-208.

606 Kiehl, J. T., and C. A. Shields, 2005: Climate simulation of the latest Permian: Implications
607 for mass extinction. *Geology*, **33**, 757-760.

608 Kiehl, J. T., C. A. Shields, J. J. Hack, and W. D. Collins, 2006: The climate sensitivity of the
609 Community Climate System Model version 3 (CCSM3). *Journal of Climate*, **19**,
610 2584-2596.

611 Kürschner, W. M., Z. Kvacek, and D. L. Dilcher, 2008: The impact of Miocene atmospheric
612 carbon dioxide fluctuations on climate and the evolution of terrestrial ecosystems.
613 *Proceedings of the National Academy of Sciences*, **105**, 449-453.

614 Kutzbach, J. E., and P. Behling, 2004: Comparison of simulated changes of climate in Asia
615 for two scenarios: Early Miocene to present, and present to future enhanced
616 greenhouse. *Global and Planetary Change*, **41**, 157-165.

617 Lagabriele, Y., Y. Godd ris, Y. Donnadieu, J. Malavieille, and M. Suarez, 2009: The
618 tectonic history of Drake Passage and its possible impacts on global climate. *Earth
619 and Planetary Science Letters*, **279**, 197-211.

620 Langebroek, P. M., A. Paul, and M. Schulz, 2009: Antarctic ice-sheet response to
621 atmospheric CO₂ and insolation in the Middle Miocene. *Clim. Past*, **5**, 633-646.

622 Larsen, H. C., 1994: Seven million years of glaciation in Greenland. *Science*, **264**, 952-955.

623 Lear, C. H., H. Elderfield, and P. A. Wilson, 2000: Cenozoic deep-sea temperatures and
624 global ice volumes from Mg/Ca in benthic foraminiferal calcite. *Science*, **287**, 269-
625 272.

626 Lorenz, D. J., and E. T. DeWeaver, 2007: Tropopause height and zonal wind response to
627 global warming in the IPCC scenario integrations. *J. Geophys. Res.*, **112**, D10119.

628 Lunt, D. J., P. J. Valdes, A. Haywood, and I. C. Rutt, 2008a: Closure of the Panama Seaway
629 during the Pliocene: Implications for climate and Northern Hemisphere glaciation.
630 *Climate Dynamics*, **30**, 1-18.

631 Lunt, D. J., G. L. Foster, A. M. Haywood, and E. J. Stone, 2008b: Late Pliocene Greenland
632 glaciation controlled by a decline in atmospheric CO₂ levels. *Nature*, **454**, 1102-1105.

633 Lunt, D. J., R. Flecker, P. J. Valdes, U. Salzmann, R. Gladstone, and A. M. Haywood, 2008c:
634 A methodology for targeting palaeo proxy data acquisition: A case study for the
635 terrestrial late Miocene. *Earth and Planetary Science Letters*, **271**, 53-62.

636 Lyle, M., 1997: Could early Cenozoic thermohaline circulation have warmed the poles?
637 *Paleoceanography*, **12**, 161-167.

638 Lyle, M., D. Wilkins, J. Barron, and L. Heusser, 2003: North Pacific Sea Surface
639 Temperature, Western U.S. Vegetation, and the Demise of the Miocene Rocky
640 Mountain Monsoon. *American Geophysical Union, Fall Meeting 2003*.

641 Lyle, M., and Coauthors, 2008: Pacific Ocean and Cenozoic evolution of climate. *Rev.*
642 *Geophys.*, **46**.

643 Meehl, G. A., J. M. Arblaster, D. M. Lawrence, A. Seth, E. K. Schneider, B. P. Kirtman, and
644 D. Min, 2006: Monsoon regimes in the CCSM3. *Journal of Climate*, **19**, 2482-2495.

645 Meehl, G. A., and Coauthors, 2007: Global Climate Projections. In: Climate Change 2007:
646 The Physical Science Basis. Contribution of Working Group I to the Fourth
647 Assessment Report of the Intergovernmental Panel on Climate Change.

648 Megirian, D., P. Murray, L. Schwartz, and C. Von Der Borch, 2004: Late Oligocene
649 Kangaroo Well Local Fauna from the Ulta Limestone (new name), and climate of the
650 Miocene oscillation across central Australia. *Australian Journal of Earth Sciences*,
651 **51**, 701-741.

652 Micheels, A., A. Bruch, and V. Mosbrugger, 2009a: Miocene climate modelling sensitivity
653 experiments for different CO₂ concentrations. *Palaeontologia Electronica*, **12**.

654 Micheels, A., J. Eronen, and V. Mosbrugger, 2009b: The Late Miocene climate response to a
655 modern Sahara desert. *Global and Planetary Change*, **67**, 193-204.

656 Micheels, A., A. A. Bruch, D. Uhl, T. Utescher, and V. Mosbrugger, 2007: A Late Miocene
657 climate model simulation with ECHAM4/ML and its quantitative validation with
658 terrestrial proxy data. *Palaeogeography, Palaeoclimatology, Palaeoecology*, **253**,
659 251-270.

660 Micheels, A., A. A. Bruch, J. Eronen, M. Fortelius, M. Harzhauser, T. Utescher, and V.
661 Mosbrugger, In Press: Analysis of heat transport mechanisms from a Late Miocene
662 model experiment with a fully-coupled atmosphere-ocean general circulation model.
663 *Palaeogeography, Palaeoclimatology, Palaeoecology*, **In Press, Corrected Proof**.

664 Miller, G., J. Mangan, D. Pollard, S. Thompson, B. Felzer, and J. Magee, 2005: Sensitivity of
665 the Australian Monsoon to insolation and vegetation: Implications for human impact
666 on continental moisture balance. *Geology*, **33**, 65-68.

667 Miller, K. G., J. D. Wright, and R. G. Fairbanks, 1991: Unlocking the ice house: Oligocene-
668 Miocene oxygen isotopes, eustasy, and margin erosion. United States, Pages: 6829-
669 6848.

670 Mix, H. T., A. Mulch, M. L. Kent-Corson, and C. P. Chamberlain, 2011: Cenozoic migration
671 of topography in the North American Cordillera. *Geology*, **39**, 87-90.

672 Moran, K., and Coauthors, 2006: The Cenozoic palaeoenvironment of the Arctic Ocean.
673 *Nature*, **441**, 601-605.

674 Mosbrugger, V., and T. Utescher, 1997: The coexistence approach -- a method for
675 quantitative reconstructions of Tertiary terrestrial palaeoclimate data using plant
676 fossils. *Palaeogeography, Palaeoclimatology, Palaeoecology*, **134**, 61-86.

677 Mosbrugger, V., T. Utescher, and D. L. Dilcher, 2005: Cenozoic continental climatic
678 evolution of Central Europe. *PNAS*, **102**, 14964-14969.

679 Müller, R. D., M. Sdrolias, C. Gaina, and W. R. Roest, 2008: Age, spreading rates and
680 spreading asymmetry of the world's ocean crust. *Geochemistry, Geophysics,*
681 *Geosystems.*, Q04006.

682 Otto-Bliesner, B. L., and G. R. Upchurch, 1997: Vegetation-induced warming of high-
683 latitude regions during the Late Cretaceous period. *Nature (London)*, **385**, 804-807.

684 Pagani, M., M. A. Arthur, and K. H. Freeman, 1999: Miocene evolution of atmospheric
685 carbon dioxide. *Paleoceanography*, **14**, 273-292.

686 Pearson, P. N., and M. R. Palmer, 2000: Atmospheric carbon dioxide concentrations over the
687 past 60 million years. *Nature*, **406**, 695-699.

688 Pekar, S. F., and R. M. DeConto, 2006: High-resolution ice-volume estimates for the early
689 Miocene: Evidence for a dynamic ice sheet in Antarctica. *Palaeogeography,*
690 *Palaeoclimatology, Palaeoecology*, **231**, 101-109.

691 Polvani, L. M., and P. J. Kushner, 2002: Tropospheric response to stratospheric perturbations
692 in a relatively simple general circulation model. *Geophys. Res. Lett.*, **29**, 1114.

- 693 Poore, H. R., R. Samworth, N. J. White, S. M. Jones, and I. N. McCave, 2006: Neogene
694 overflow of Northern Component Water at the Greenland-Scotland Ridge. *Geochem.*
695 *Geophys. Geosyst.*, **7**, Q06010.
- 696 Potter, P. E., and P. Szatmari, 2009: Global Miocene tectonics and the modern world. *Earth-*
697 *Science Reviews*, **96**, 279-295.
- 698 Prell, W. L., and J. E. Kutzbach, 1992: Sensitivity of the Indian monsoon to forcing
699 parameters and implications for its evolution. *Nature*, **360**, 647-652.
- 700 Ramsay, A. T. S., C. W. Smart, and J. C. Zachos, 1998: A model of early to middle Miocene
701 deep ocean circulation for the Atlantic and Indian oceans. *Geological evolution of*
702 *ocean basins; results from the Ocean Drilling Program*, A. Cramp, C. J. MacLeod, S.
703 V. Lee, and E. J. W. Jones, Eds., Geological Society of London, 55-70.
- 704 Randel, W. J., F. Wu, H. Vömel, G. E. Nedoluha, and P. Forster, 2006: Decreases in
705 stratospheric water vapor after 2001: Links to changes in the tropical tropopause and
706 the Brewer-Dobson circulation. *J. Geophys. Res.*, **111**, D12312.
- 707 Retallack, G. J., 2001: A 300-million-year record of atmospheric carbon dioxide from fossil
708 plant cuticles. *Nature*, **411**, 287-290.
- 709 ———, 2004: Late Miocene climate and life on land in Oregon within a context of Neogene
710 global change. *Palaeogeography, Palaeoclimatology, Palaeoecology*, **214**, 97-123.
- 711 ———, 2009: Refining a pedogenic-carbonate CO₂ paleobarometer to quantify a middle
712 Miocene greenhouse spike. *Palaeogeography, Palaeoclimatology, Palaeoecology*,
713 **281**, 57-65.
- 714 Rind, D., D. Shindell, P. Lonergan, and N. K. Balachandran, 1998: Climate Change and the
715 Middle Atmosphere. Part III: The Doubled CO₂ Climate Revisited. *Journal of*
716 *Climate*, **11**, 876-894.

- 717 Rind, D., M. Chandler, P. Lonergan, and J. Lerner, 2001: Climate change and the middle
718 atmosphere 5. Paleostratosphere in cold and warm climates. *Journal of Geophysical*
719 *Research D: Atmospheres*, **106**, 20195-20212.
- 720 Rögl, F., 1999: Mediterranean and Paratethys; facts and hypotheses of an Oligocene to
721 Miocene paleogeography; short overview. *Geologica Carpathica (Bratislava)*, **50**,
722 339-349.
- 723 Rosenfield, J. E., 1993: Radiative feedback of polar stratospheric clouds on Antarctic
724 temperatures. *Geophys. Res. Lett.*, **20**, 1195-1198.
- 725 Rowley, D. B., and B. S. Currie, 2006: Palaeo-altimetry of the late Eocene to Miocene
726 Lunpola basin, central Tibet.
- 727 Ruddiman, W. F., and J. E. Kutzbach, 1989: Forcing of Late Cenozoic Northern Hemisphere
728 Climate by Plateau Uplift in Southern Asia and the American West. *J. Geophys. Res.*,
729 **94**, 18409-18427.
- 730 Ruddiman, W. F., J. E. Kutzbach, and I. C. Prentice, 1997: Testing the climatic effects of
731 orography and CO₂ with general circulation and biome models. *Tectonic uplift and*
732 *climate change*, W. F. Ruddiman, Ed., Plenum Press, 203-235.
- 733 Schnitker, D., 1980: North Atlantic oceanography as possible cause of Antarctic glaciation
734 and eutrophication. *Nature*, **284**, 615-616.
- 735 Sheldon, N. D., 2006: Using paleosols of the Picture Gorge Basalt to reconstruct the middle
736 Miocene climatic optimum. University of California, Museum of Paleontology, 27-
737 36.
- 738 Shellito, C. J., and L. C. Sloan, 2006: Reconstructing a lost Eocene Paradise, Part II: On the
739 utility of dynamic global vegetation models in pre-Quaternary climate studies. *Global*
740 *and Planetary Change*, **50**, 18-32.

- 741 Shellito, C. J., J.-F. Lamarque, and L. C. Sloan, 2009: Early Eocene Arctic climate sensitivity
742 to pCO₂ and basin geography. *Geophys. Res. Lett.*, **36**.
- 743 Shevenell, A. E., J. P. Kennett, and D. W. Lea, 2008: Middle Miocene ice sheet dynamics,
744 deep-sea temperatures, and carbon cycling: A Southern Ocean perspective. *Geochem.*
745 *Geophys. Geosyst.*, **9**.
- 746 Sijp, W. P., and M. H. England, 2004: Effect of the Drake Passage Throughflow on Global
747 Climate. *Journal of Physical Oceanography*, **34**, 1254-1266.
- 748 Sloan, L. C., and D. Pollard, 1998: Polar stratospheric clouds: A high latitude warming
749 mechanism in an ancient greenhouse world. *Geophysical Research Letters*, **25**, 3517-
750 3520.
- 751 Sloan, L. C., J. C. G. Walker, and T. C. Moore Jr, 1995: Possible role of oceanic heat
752 transport in early Eocene climate. *Paleoceanography*, **10**, 347-356.
- 753 Sluiter, I. R. K., A. P. Kershaw, G. R. Holdgate, and D. Bulman, 1995: Biogeographic,
754 ecological and stratigraphic relationships of the Miocene brown coal floras, Latrobe
755 Valley, Victoria, Australia. *International Journal of Coal Geology*, **28**, 277-302.
- 756 Spicer, R. A., and Coauthors, 2003: Constant elevation of southern Tibet over the past 15
757 million years. *Nature*, **421**, 622-624.
- 758 Stan, C., and Coauthors, 2010: An ocean-atmosphere climate simulation with an embedded
759 cloud resolving model. *Geophys. Res. Lett.*, **37**.
- 760 Steppuhn, A., A. Micheels, G. Geiger, and V. Mosbrugger, 2006: Reconstructing the Late
761 Miocene climate and oceanic heat flux using the AGCM ECHAM4 coupled to a
762 mixed-layer ocean model with adjusted flux correction. *Palaeogeography,*
763 *Palaeoclimatology, Palaeoecology*, **238**, 399-423.

- 764 Steppuhn, A., A. Micheels, A. Bruch, D. Uhl, T. Utescher, and V. Mosbrugger, 2007: The
765 sensitivity of ECHAM4/ML to a double CO₂ scenario for the Late Miocene and the
766 comparison to terrestrial proxy data. *Global and Planetary Change*, **57**, 189-212.
- 767 Sun, Q.-G., M. E. Collinson, C.-S. Li, Y.-F. Wang, and D. J. Beerling, 2002: Quantitative
768 reconstruction of palaeoclimate from the Middle Miocene Shanwang flora, eastern
769 China. *Palaeogeography, Palaeoclimatology, Palaeoecology*, **180**, 315-329.
- 770 Syabryaj, S., T. Utescher, S. Molchanoff, and A. A. Bruch, 2007: Vegetation and
771 palaeoclimate in the Miocene of Ukraine. *Palaeogeography, Palaeoclimatology,*
772 *Palaeoecology*, **253**, 169-184.
- 773 Tong, J. A., Y. You, R. D. Müller, and M. Seton, 2009: Climate model sensitivity to
774 atmospheric CO₂ concentrations for the middle Miocene. *Global and Planetary*
775 *Change*, **67**, 129-140.
- 776 Tripathi, A. K., C. D. Roberts, and R. A. Eagle, 2009: Coupling of CO₂ and Ice Sheet Stability
777 Over Major Climate Transitions of the Last 20 Million Years. *Science*, **326**, 1394-
778 1397.
- 779 Uhl, D., V. Mosbrugger, A. Bruch, and T. Utescher, 2003: Reconstructing
780 palaeotemperatures using leaf floras - case studies for a comparison of leaf margin
781 analysis and the coexistence approach. *Review of Palaeobotany and Palynology*, **126**,
782 49-64.
- 783 Uhl, D., A. A. Bruch, C. Traiser, and S. Klotz, 2006: Palaeoclimate estimates for the Middle
784 Miocene Schrotzburg flora (S Germany): A multi-method approach. *International*
785 *Journal of Earth Sciences*, **95**, 1071-1085.
- 786 Uhl, D., S. Klotz, C. Traiser, C. Thiel, T. Utescher, E. Kowalski, and D. L. Dilcher, 2007:
787 Cenozoic paleotemperatures and leaf physiognomy -- A European perspective.
788 *Palaeogeography, Palaeoclimatology, Palaeoecology*, **248**, 24-31.

- 789 Utescher, T., V. Mosbrugger, and A. R. Ashraf, 2000: Terrestrial Climate Evolution in
790 Northwest Germany Over the Last 25 Million Years. *Palaios*, **15**, 430-449.
- 791 Utescher, T., D. Djordjevic-Milutinovic, A. Bruch, and V. Mosbrugger, 2007: Palaeoclimate
792 and vegetation change in Serbia during the last 30 Ma. *Palaeogeography,*
793 *Palaeoclimatology, Palaeoecology*, **253**, 157-168.
- 794 von der Heydt, A., and H. A. Dijkstra, 2006: Effect of ocean gateways on the global ocean
795 circulation in the late Oligocene and early Miocene. *Paleoceanography*, **21**, PA1011.
- 796 Wang, C., and Coauthors, 2008: Constraints on the early uplift history of the Tibetan Plateau.
797 *Proceedings of the National Academy of Sciences*, **105**, 4987-4992.
- 798 White, J. M., and T. A. Ager, 1994: Palynology, paleoclimatology and correlation of Middle
799 Miocene beds from Porcupine River (locality 90-1), Alaska. *Quaternary*
800 *International*, **22-23**, 43-77.
- 801 Wiemann, M. C., S. R. Manchester, and E. A. Wheeler, 1999: Paleotemperature estimation
802 from dicotyledonous wood anatomical characters. *Palaios*, **14**, 459-474.
- 803 Willmott, C. J., and K. Matsuura: Terrestrial Air Temperature and Precipitation: Monthly and
804 Annual Time Series (1950 - 1999). [Available online at
805 <http://climate.geog.udel.edu/~climate.>]
- 806 Wolfe, J. A., 1985: Distribution of major vegetational types during the Tertiary. *Geophysical*
807 *Monograph*, E. T. Sundquist, and W. S. Broecker, Eds., American Geophysical
808 Union, 357-375.
- 809 ———, 1994a: Tertiary climatic changes at middle latitudes of western North America.
810 *Palaeogeography, Palaeoclimatology, Palaeoecology*, **108**, 195-205.
- 811 Wolfe, J. A., 1994b: An analysis of Neogene climates in Beringia. *Palaeogeography,*
812 *Palaeoclimatology, Palaeoecology*, **108**, 207-216.

- 813 Woodruff, F., and S. M. Savin, 1989: Miocene deepwater oceanography. *Paleoceanography*,
814 **4**, 87-140.
- 815 Wright, J. D., and K. G. Miller, 1996: Control of North Atlantic Deep Water circulation by
816 the Greenland- Scotland Ridge. *Paleoceanography*, **11**, 157-170.
- 817 Yang, J., Y.-F. Wang, R. A. Spicer, V. Mosbrugger, C.-S. Li, and Q.-G. Sun, 2007: Climatic
818 reconstruction at the Miocene Shanwang basin, China, using leaf margin analysis,
819 CLAMP, coexistence approach, and overlapping distribution analysis. 599-608.
- 820 Yeager, S. G., C. A. Shields, W. G. Large, and J. J. Hack, 2006: The low-resolution CCSM3.
821 *Journal of Climate*, **19**, 2545-2566.
- 822 Yin, J. H., 2005: A consistent poleward shift of the storm tracks in simulations of 21st
823 century climate. *Geophys. Res. Lett.*, **32**, L18701.
- 824 You, Y., M. Huber, R. D. Müller, C. J. Poulsen, and J. Ribbe, 2009: Simulation of the Middle
825 Miocene Climate Optimum. *Geophys. Res. Lett.*, **36**, L04702.
- 826 Zachos, J., M. Pagani, L. Sloan, E. Thomas, and K. Billups, 2001: Trends, rhythms, and
827 aberrations in global climate 65 Ma to present. *Science*, **292**, 686-693.
- 828 Zachos, J. C., G. R. Dickens, and R. E. Zeebe, 2008: An early Cenozoic perspective on
829 greenhouse warming and carbon-cycle dynamics. *Nature*, **451**, 279-283.
- 830 Zhao, L.-C., Y.-F. Wang, C.-J. Liu, and C.-S. Li, 2004: Climatic implications of fruit and
831 seed assemblage from Miocene of Yunnan, southwestern China. *Quaternary*
832 *International*, **117**, 81-89.
- 833 Zhongshi, Z., H. Wang, Z. Guo, and D. Jiang, 2007a: What triggers the transition of
834 palaeoenvironmental patterns in China, the Tibetan Plateau uplift or the Paratethys
835 Sea retreat? *Palaeogeography, Palaeoclimatology, Palaeoecology*, **245**, 317-331.

836 Zhongshi, Z., W. Huijun, G. Zhengtang, and J. Dabang, 2007b: Impacts of tectonic changes
837 on the reorganization of the Cenozoic paleoclimatic patterns in China. *Earth and*
838 *Planetary Science Letters*, **257**, 622-634.

839

840

841 Figure 1. Topography and bathymetry for the Miocene (a) and control case (b). Terrestrial
842 temperature and precipitation proxies indicated by red triangles (Tables 2 and 3). L-M
843 indicates Lago-Mare.

844 Figure 2. Zonal mean surface temperature (a) and land temperature (b) for the Miocene
845 (solid) and control case (dashed). Dotted line indicates anomaly (right axis).

846 Figure 3. Control case surface temperatures for June-July-August, December-January-
847 February and the annual mean (a-c). Miocene – control case surface temperature anomalies (d
848 -f).

849 Figure 4. Zonal atmospheric temperature for the control case during June-July-August (a) and
850 December-January-February (b). Miocene – control case anomalies (c and d).

851 Figure 5. Same as figure 4 except for zonal wind.

852 Figure 6. Same as figure 4 except for eddy kinetic energy.

853 Figure 7. Annual meridional overturning circulation for the control case (a) and the Miocene
854 – control case anomaly (b).

855 Figure 8. Precipitation for the Miocene (a-c) and control case (d-f) for June-July-August
856 (JJA), December-January-February (DJF) and DJF-JJA anomalies.

857 Figure 9. Same as figure 8 except for surface wind.

858 Figure 10. Ocean (red) and atmosphere (blue) heat transport for the Miocene (solid) and
859 control case (dashed).

860 Figure 11. Residual surface energy flux for the Miocene (solid line) and control case (dashed
861 line). Dotted line indicates anomaly (right axis).

862

Figure 1. Topography and bathymetry for the Miocene (a) and control case (b). Terrestrial temperature and precipitation proxies indicated by red triangles (Tables 2 and 3). L-M indicates Lago-Mare.

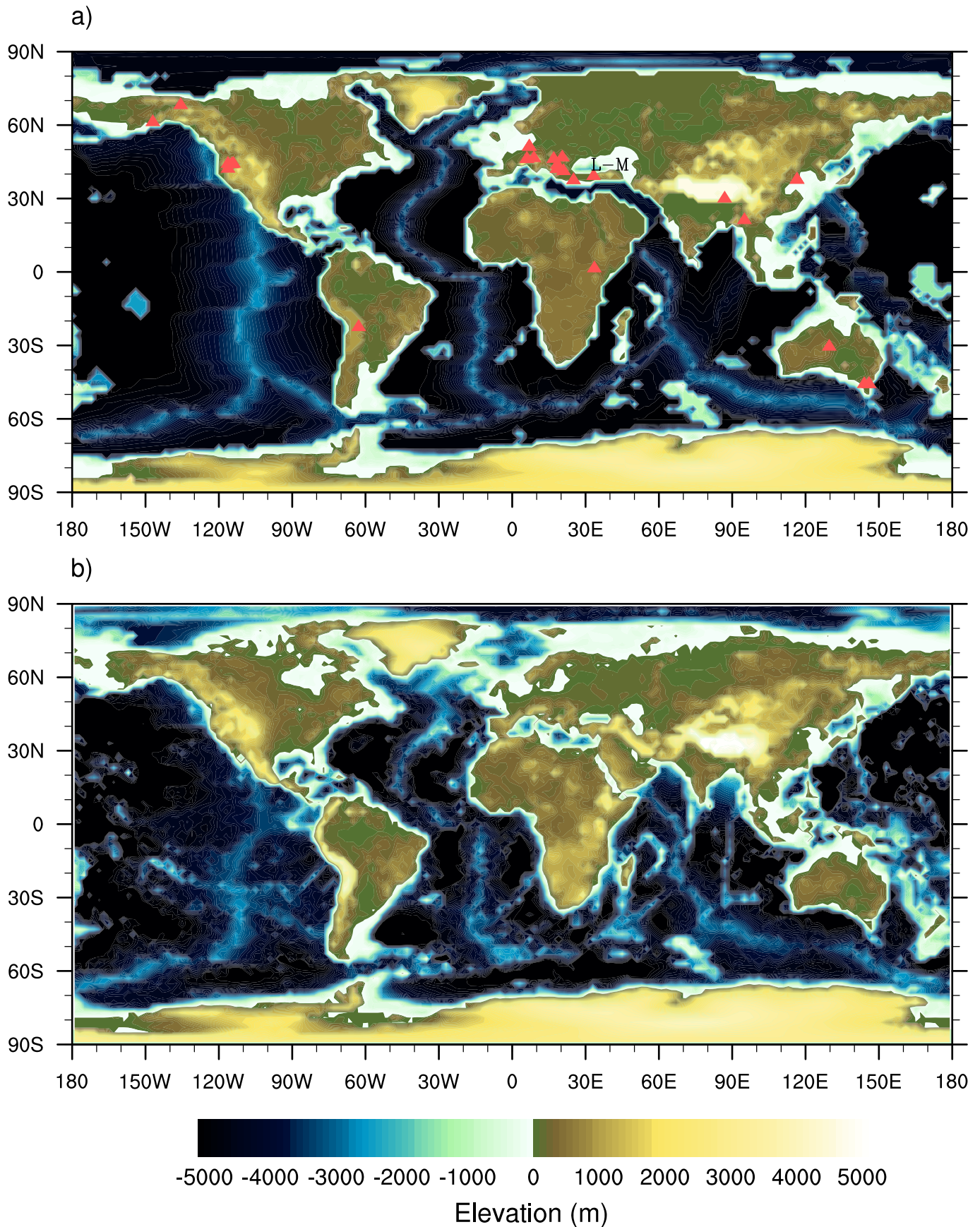


Figure 2. Zonal mean surface temperature (a) and land temperature (b) for the Miocene (solid line) and control case (dashed line). Dotted line indicates anomaly (right axis).

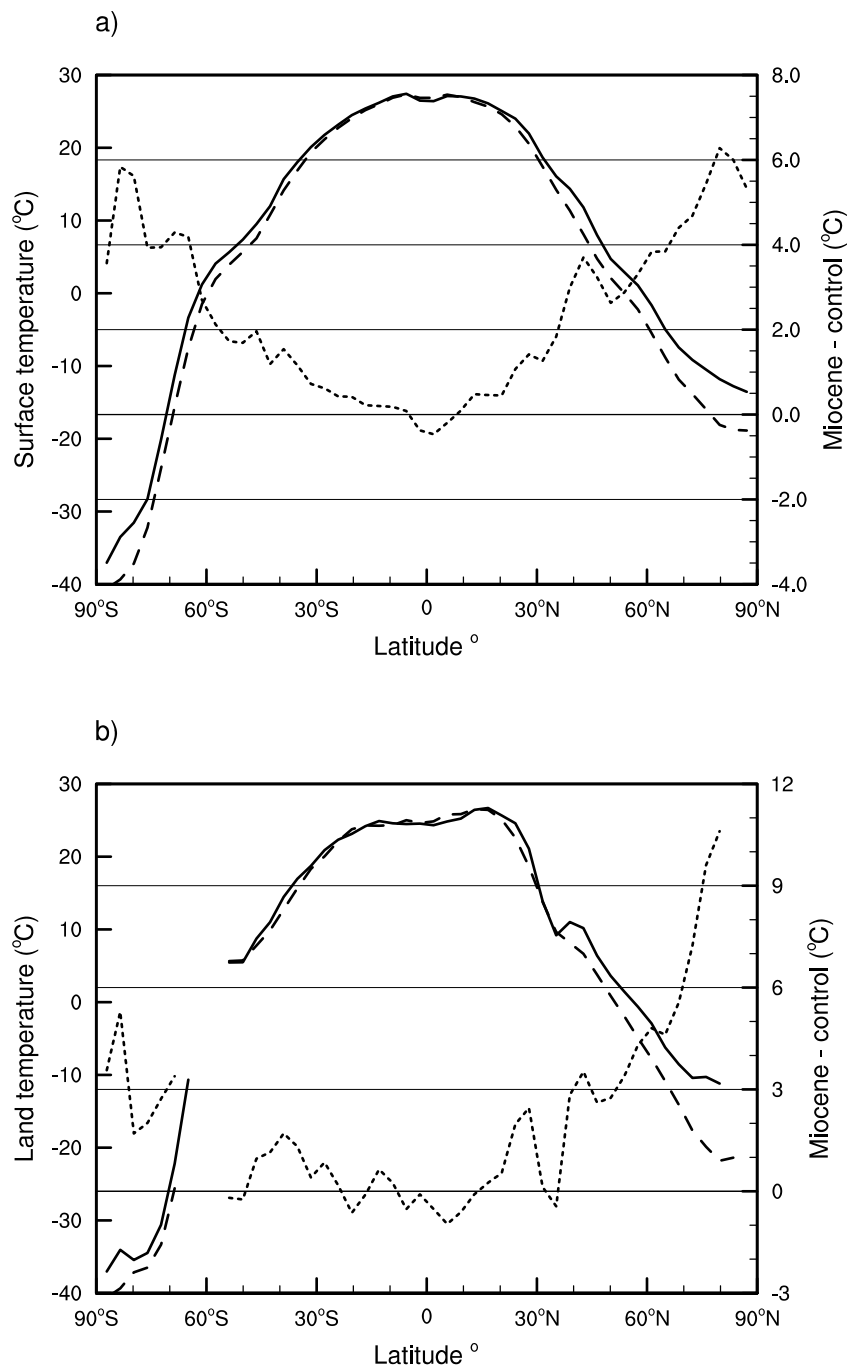


Figure 3. Control case surface temperatures for June-July-August, December-January-February and the annual mean (a-c). Miocene - control case surface temperature anomalies (d-f).

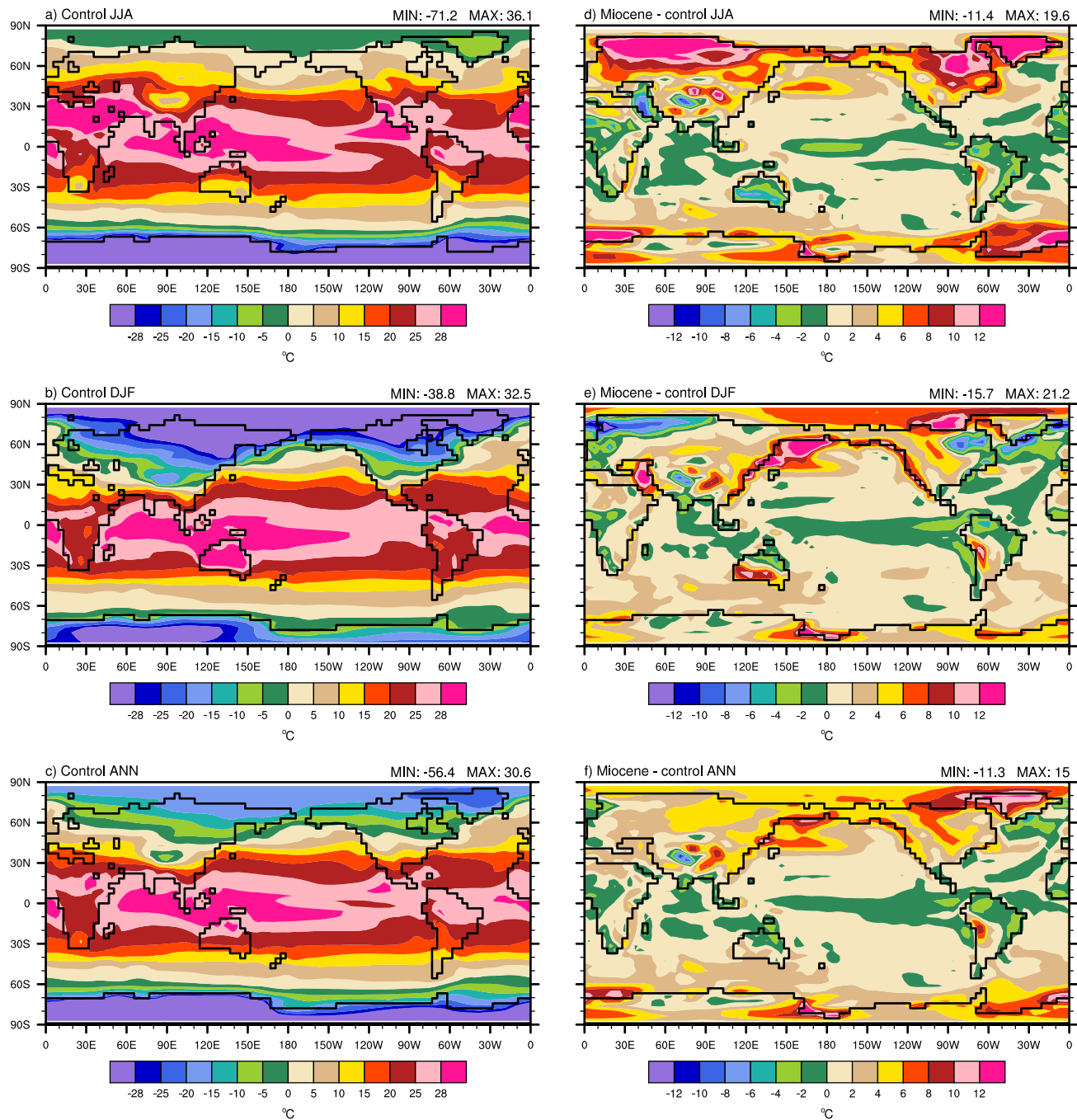


Figure 4. Zonal atmospheric temperature for the control case during June-July-August (a) and December-January-February (b). Miocene - control case temperature anomalies (c-d).

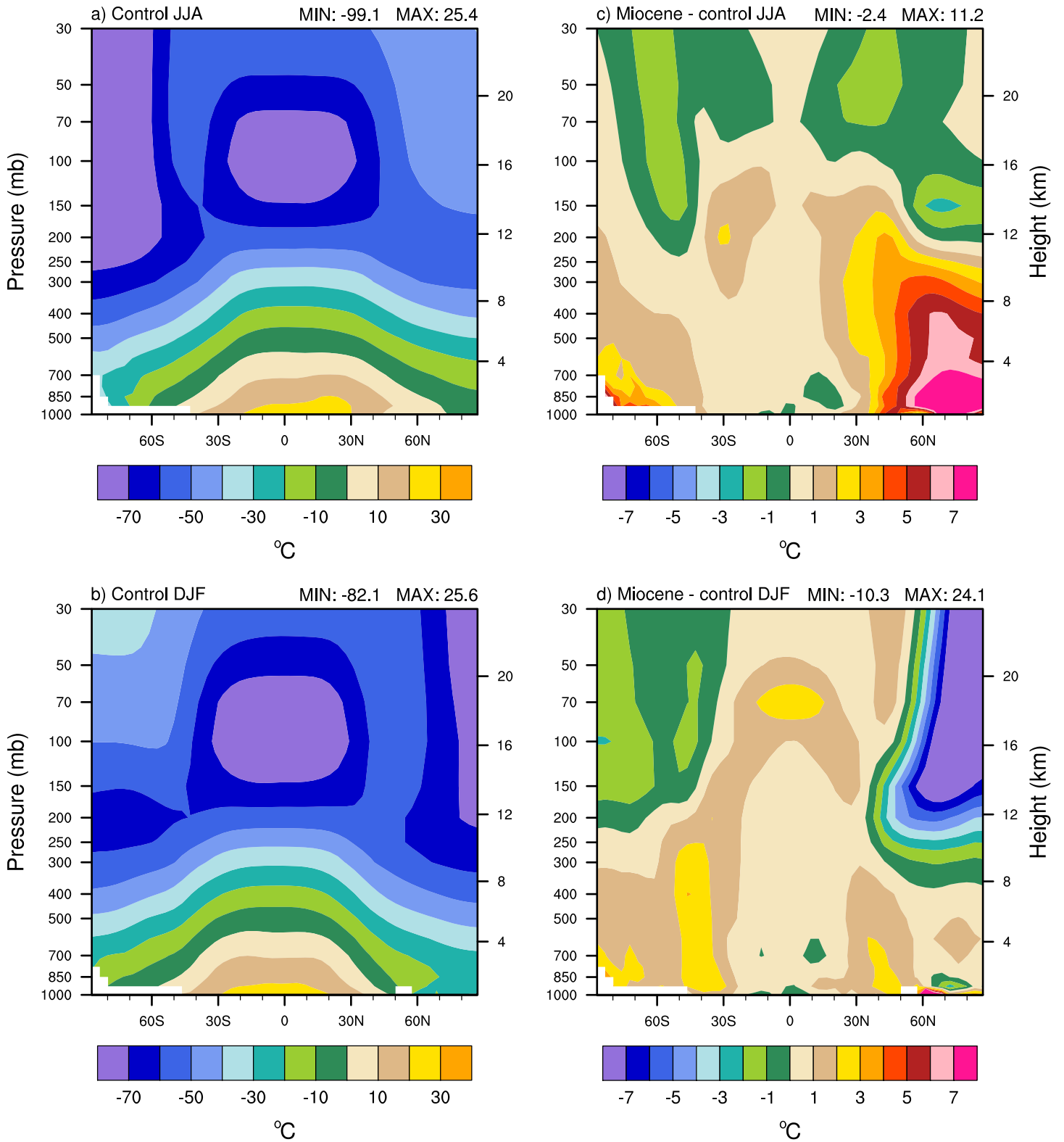


Figure 5. Same as figure 4 except for zonal wind.

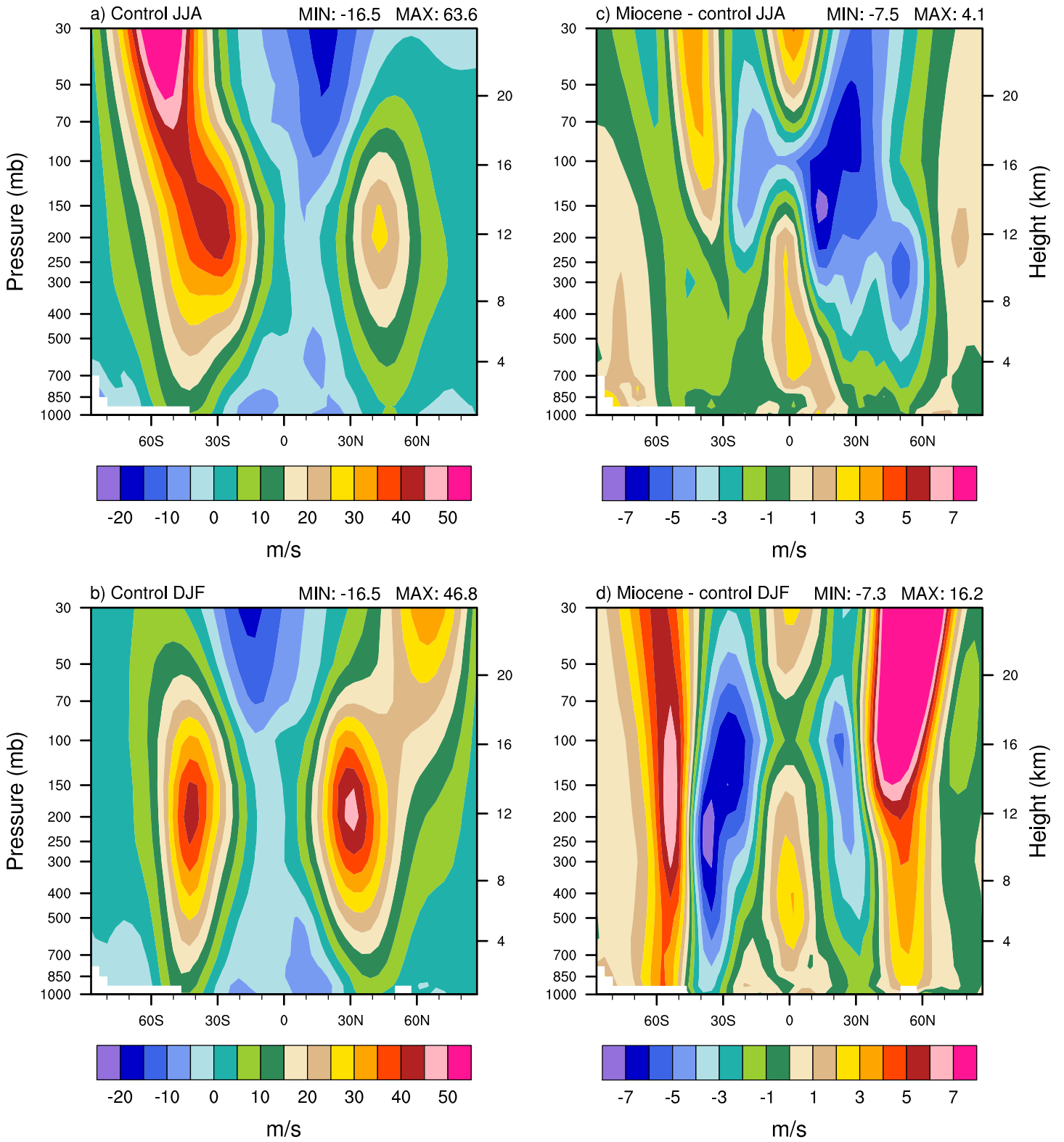


Figure 6. Same as figure 4 except for eddy kinetic energy.

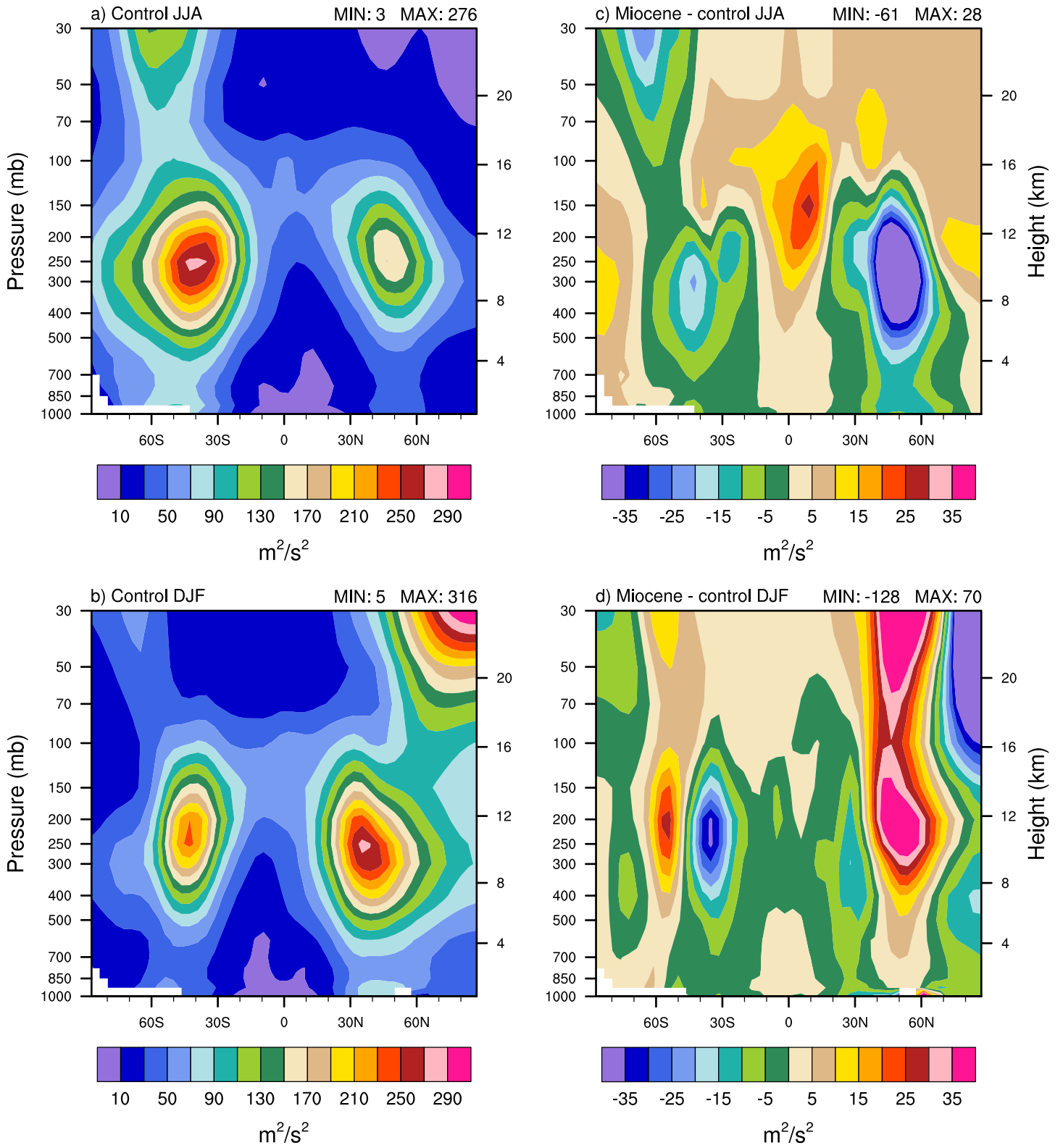


Figure 7. Annual meridional overturning circulation for the control case (a) and the Miocene - control case anomaly (b).

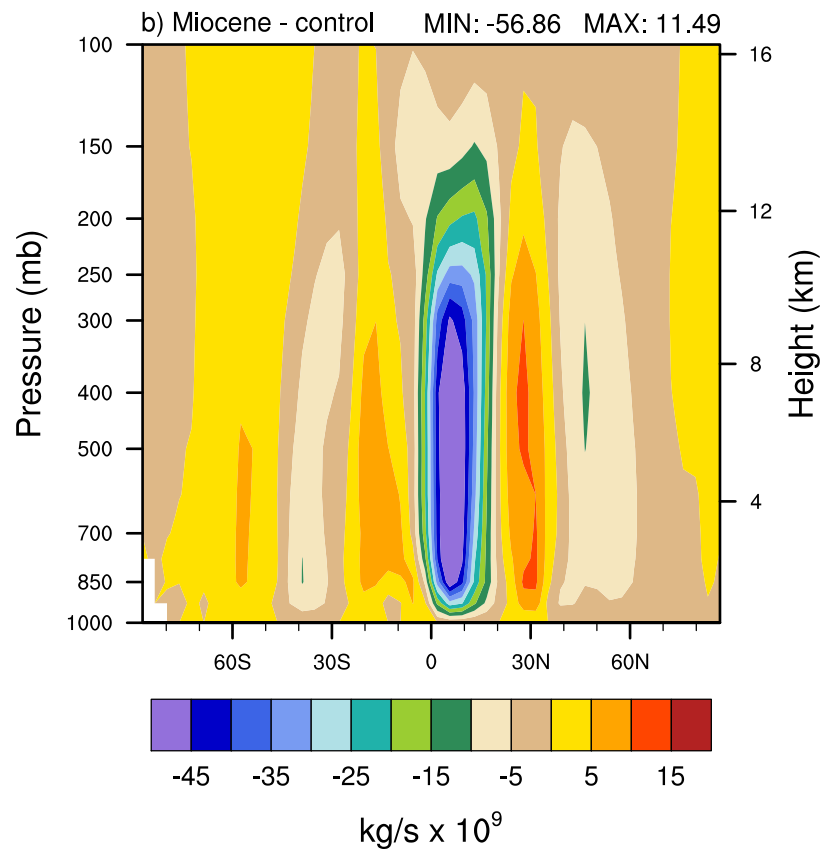
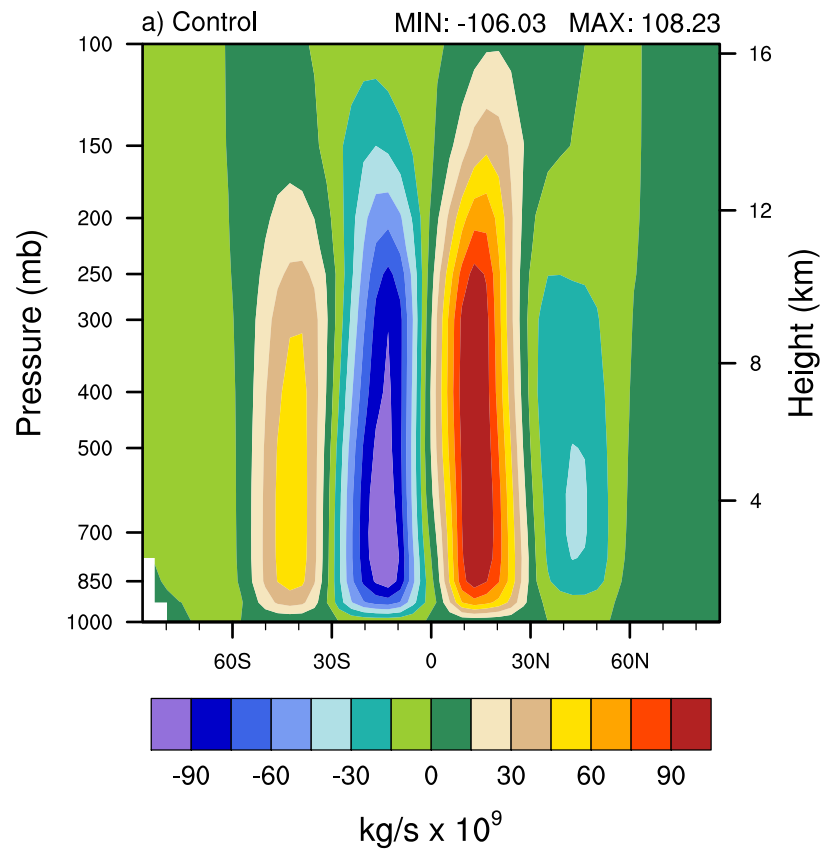


Figure 8. Precipitation for the Miocene (a-c) and control case (d-f) for June-July-August (JJA), December-January-February (DJF) and DJF-JJA anomalies.

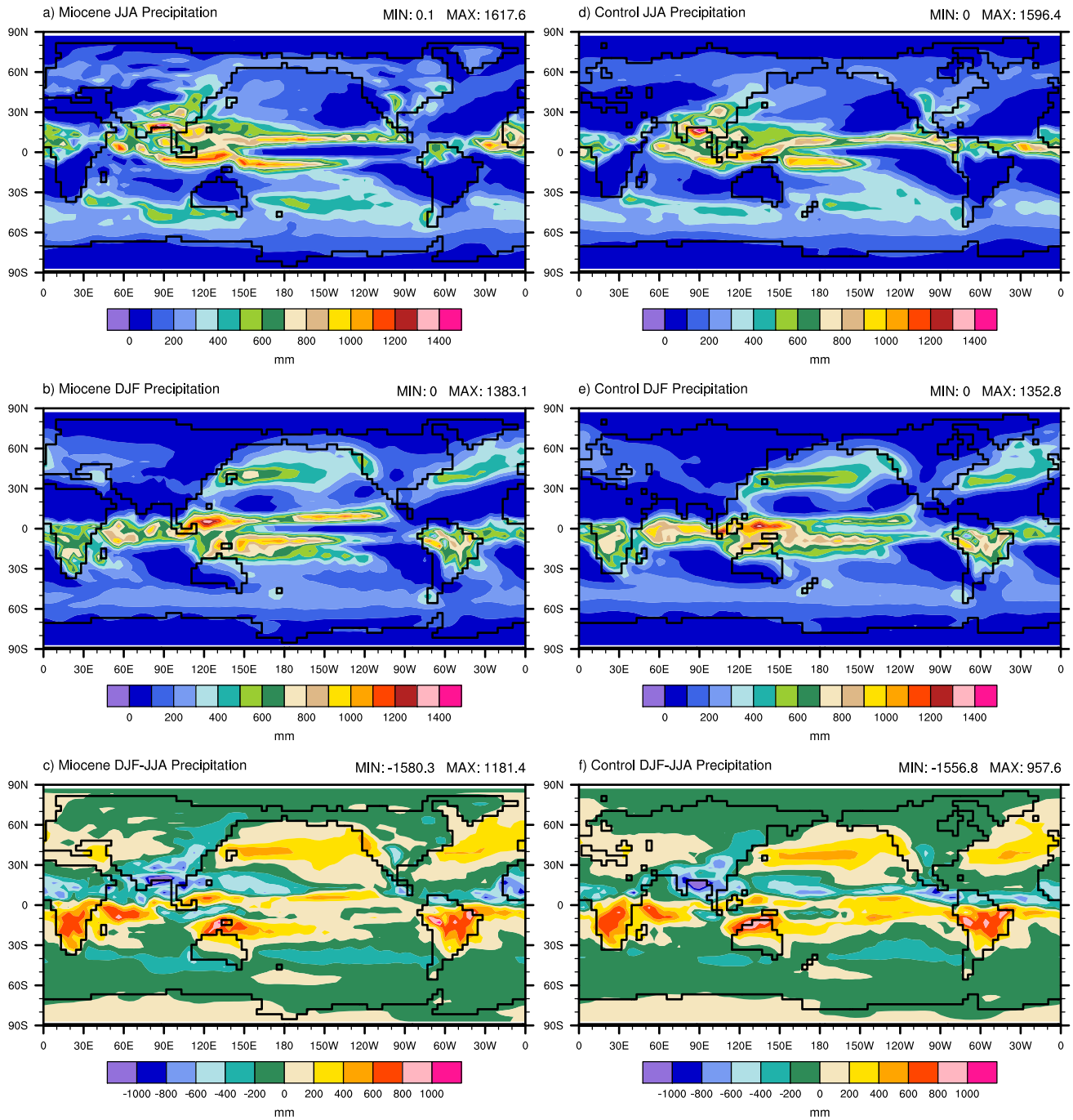


Figure 9. Same as figure 8 except for surface wind.

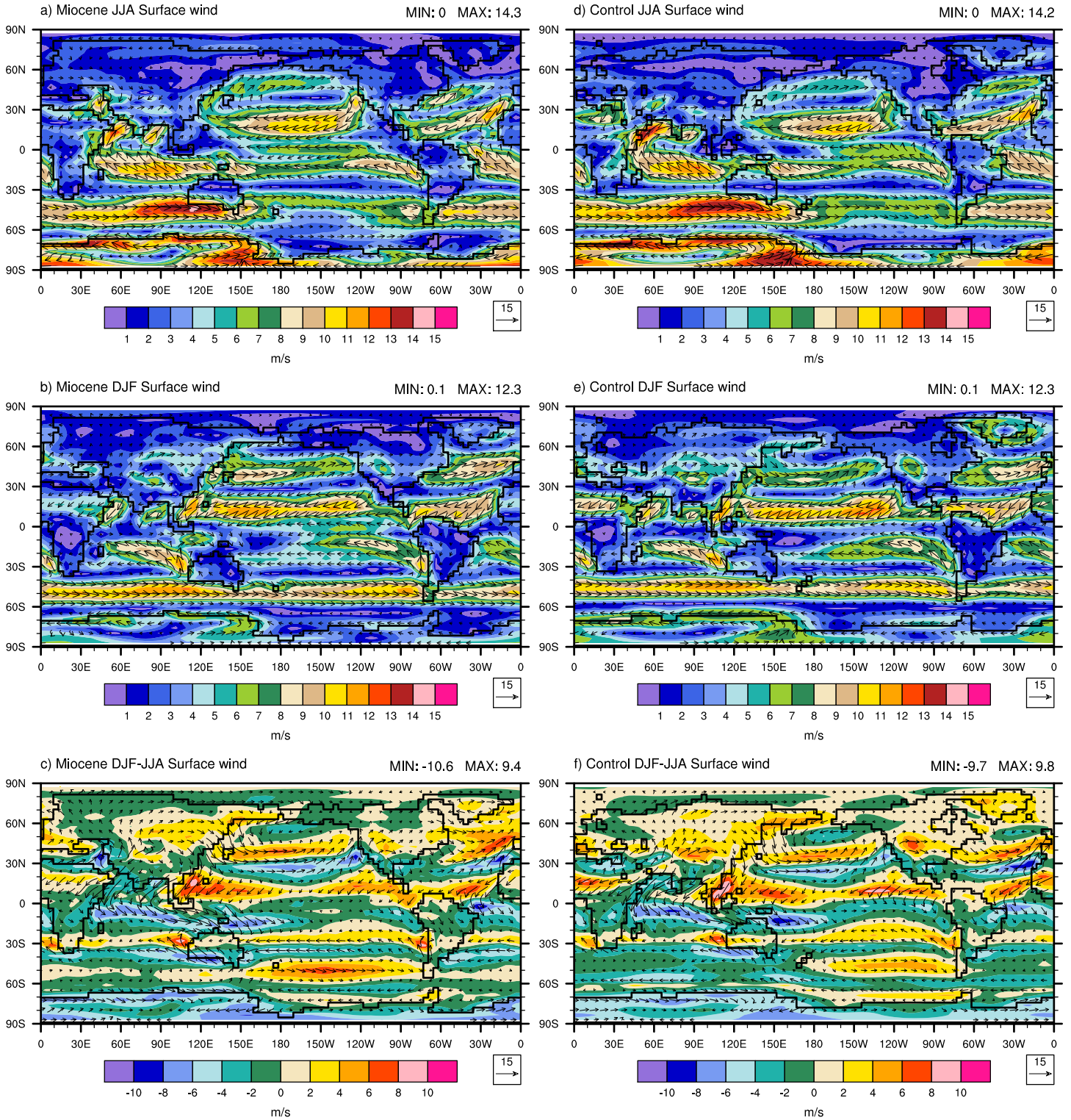


Figure 10. Ocean (red) and atmosphere (blue) heat transport for the Miocene (solid) and control case (dashed).

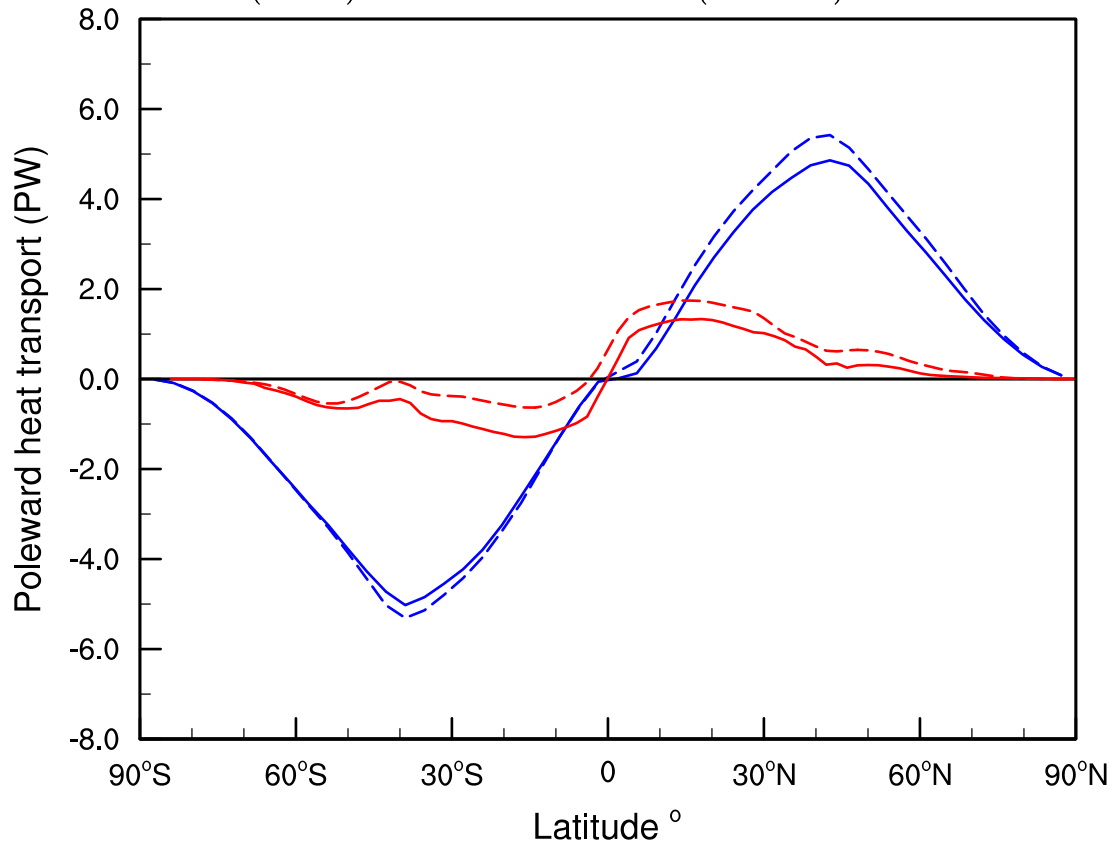


Figure 11. Residual surface energy flux for the Miocene (solid line) and control case (dashed line). Dotted line indicates anomaly (right axis).

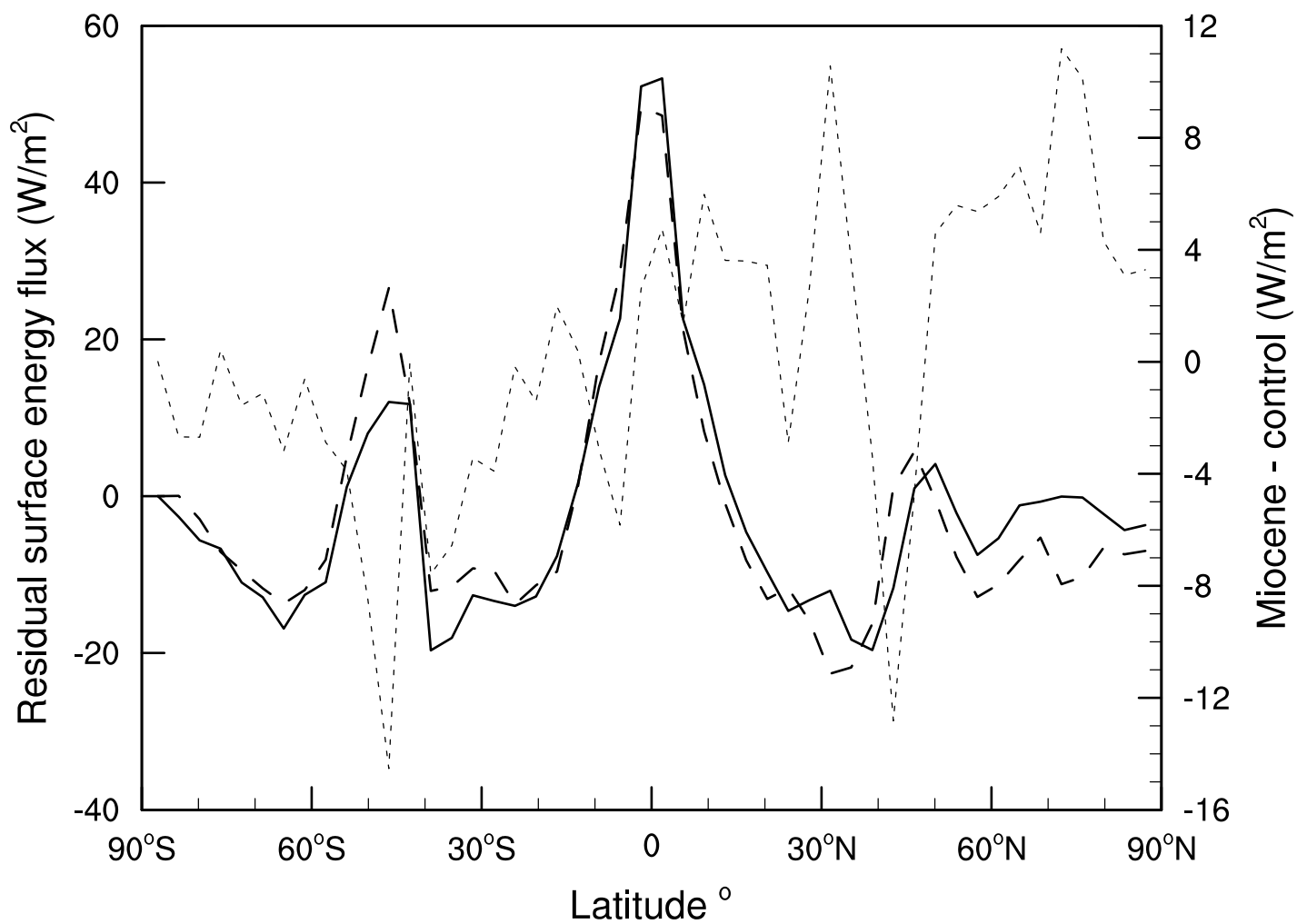


Table 1. Global mean CCSM3 diagnostics.

	Miocene	Control
Residual top of model energy flux (W/m^2)	-0.086	0.023
Residual surface energy flux (W/m^2)	-0.109	0.003
Surface temperature ($^{\circ}C$)	15.38	13.88
Surface temperature – land only ($^{\circ}C$)	8.70	7.41
Surface albedo	0.11	0.15
Cumulative precipitation (mm/year)	104	99
Net shortwave radiation at surface (W/m^2)	163.5	158.6
Net longwave radiation at surface (W/m^2)	57.9	57.8
Sensible heat flux (W/m^2)	22.6	21.6
Latent heat flux (W/m^2)	83.1	79.2

Table 2. Temperature change simulated by the CCSM3 versus change between modern observations and proxy records.

Location	Paleo Lon/Lat ^a	Control case 2 meter air temp (°C)	Miocene case 2 meter air temp (°C)	Simulated warming (°C) ^b	Modern observed 2 meter air temp (°C) ^c	Miocene proxy temp (°C) ^d	Proxy derived warming (°C) ^e	Ref
Weisselster and Lausitz Basin, NE Germany	7/52	5.5	7.3	1.8	8.6	18	9.4	1
Lower Rhine Embayment, NW Germany	7/52	5.5	7.3	1.8	8.6	18.25	9.7	2
Schrotzberg, Southern Germany	6/47	8.8	7.4	-1.4	8.5	15.5	7.0	3
NW Bulgaria	21/42	11.5	13.6	2.1	6.8	17	10.2	4
Lower Rhine Embayment, NW Germany	7/52	5.5	7.3	1.8	8.6	15.95	7.4	5
Schrotzberg, Southern Germany	6/47	8.8	7.4	-1.4	8.5	15.45	7.0	6
Kovago-old al	17/47	8.1	9.0	0.9	10.4	18.65	8.2	7
Southern Germany (see ref for locations)	8.9/47.3	8.2	7.4	-0.8	8.0	18.95	10.9	8
Ukraine	20.5/47.6	8.1	9.0	0.9	10.0	17	7.0	9
Bigadic, Turkey	25.1/38.3	14.9	16.7	1.8	12.9	19.25	6.3	10
Samsun-Havza, Turkey	33.3/40	11.8	14.6	2.8	8.5	19	10.5	10
Pannonian Basin	18.5/44.55	7.8	11.8	4.0	10.4	15.25	4.8	11
Popovac, Serbia	18.3/42.9	11.5	11.8	0.3	8.9	17.85	8.9	12
Latrobe Valley, SE Australia	146/-45	12.8	11.0	-1.8	14.2	19	4.8	13
Bacchus Marsh, SE Australia	144/-45	15.7	10.8	-4.9	13.0	13	0.0	14
Yallourn, SE Australia	146/-45	12.8	11.0	-1.8	14.2	15.5	1.3	15
Kangaroo Well, Central Australia	129.7/-29.7	23.9	20.7	-3.2	21.2	17	-4.2	16
Yunnan Province, SW China	95/22	23.0	23.7	0.7	23.1	19.65	-3.5	17
Shanwang, China	116.5/38.5	8.4	10.1	1.7	12.8	16.25	3.4	18
Shanwang, China	116.5/38.5	8.4	10.1	1.7	12.8	12.7	-0.1	19
Shanwang, China	116.5/38.5	8.4	10.1	1.7	12.8	10.35	-2.5	20
Namling Basin, Southern Tibet	86.9/30.8	-5.1	-1.8	3.3	-2.3	6.8	9.1	21
Picture Gorge Subgroup, North America	-114.7/44.8	3.4	6.8	3.4	7.1	12	4.9	22
Eastern Oregon, North America	-114/45	3.4	5.3	2.0	7.1	12.7	5.6	23
Alaska, North America	-135.6/69	-11.3	-6.8	4.4	-7.7	9	16.7	24
Cape Blanco, North America	-116.3/45	9.1	7.4	-1.7	7.1	16.6	9.5	25
Waeaverville, North America	-116.3/43	6.1	9.3	3.2	7.3	16.2	8.9	25
Cook Inlet, North America	-147/62	-6.7	-0.1	6.6	2.4	11.2	8.8	26
Potosi, Bolivia	-62.8/-21.7	16.8	24.9	8.1	12.3	21.6	9.3	27
Fejej, Ethiopia	33.6/2.3	23.0	24.3	1.3	28.9	26	-2.9	28
			MEAN:	1.3			5.9	

NOTE: Proxy records from Herold et al. (2010).

^a Where paleo coordinates are not provided by reference values are calculated using modern coordinates, a plate kinematic model and the rotations of Müller et al. (2008).

^b Column three subtracted from column four.

^c Uses the dataset of Willmott and Matsuura (2001) for 2 meter air temperature spanning 1950 - 1999.

^d Where a range of values is given, the midpoint is used.

^e Column six subtracted from column seven.

^f References – 1) Mosbrugger et al. (2005), 2) Utescher et al. (2000), 3) Uhl et al. (2006), 4) Ivanov et al. (2002), 5) Mosbrugger and Utescher (1997), 6) Uhl et al. (2003), 7) Uhl et al. (2007), 8) Bohme et al. (2007), 9) Syabryaj et al. (2007), 10) Akgun et al. (2007), 11) Erdei et al. (2007), 12) Utescher et al. (2007), 13) Sluiter et al. (1995), 14) Greenwood (1994), 15) Kemp (1978), 16) Megirian et al. (2004), 17) Zhao et al. (2004), 18) Liang et al. (2003), 19) Yang et al. (2007), 20) Sun et al. (2002), 21) Spicer et al. (2003), 22) Sheldon (2006), 23) Retallack (2004), 24) White and Ager (1994), 25) Wolfe (1994b), 26) Wolfe (1994), 27) Gregory-Wodzicki et al. (1998), 28) Wiemann et al. (1999).

Table 3. Precipitation change simulated by the CCSM3 versus change between modern observations and proxy records.

Location	Paleo Lon/Lat ^a	Control case precipitation (mm)	Miocene case precipitation (mm)	Simulated precipitation change (mm) ^b	Modern observed precipitation (mm) ^c	Miocene proxy precipitation (mm) ^d	Proxy derived precipitation change (mm) ^e	Ref ^f
Weisselster and Lausitz Basin NE Germany	7/52	771.8	942.9	171.1	685.7	1300	614.3	1
Lower Rhine Embayment, NW Germany	7/52	771.8	942.9	171.1	685.7	1350	664.3	2
Schrotzberg, Southern Germany	6/47	813.7	1154.1	340.4	1109	1300	191	3
NW Bulgaria	21/42	504.7	568.1	63.4	693.7	1200	506.3	4
Lower Rhine Embayment, NW Germany	7/52	771.8	942.9	171.1	685.7	1293	607.3	5
Southern Germany (see ref for locations)	8.9/47.3	807.1	1154.1	347.0	1222.4	1146	-76.9	8
Ukraine	20.5/47.6	609.0	941.5	332.6	588.5	1168	579	9
Bigadic, Turkey	25.1/38.3	391.4	436.7	45.3	758.7	1270	510.8	10
Samsun-Havza, Turkey	33.3/40	374.6	648.7	274.1	413	1270	856.5	10
Pannonian Basin	18.5/44.6	714.1	664.9	-49.2	550.2	1074	523.8	11
Popovac, Serbia	18.3/42.9	504.7	664.9	160.2	789.3	1434	644.7	12
Latrobe Valley, SE Australia	146/-45	375.0	798.1	423.1	832.2	1700	867.8	13
Yallourn, SE Australia	146/-45	375.0	798.1	423.1	832.2	1500	667.8	15
Kangaroo Well, Central Australia	129.7/-29.7	387.8	448.8	61.0	237.1	450	212.9	16
Yunnan Province, SW China	95/22	566.7	2167.4	1600.7	1136.1	1235	98.9	17
Shanwang, China	116.5/38.5	1056.2	1107.0	50.7	725.4	1139	413.1	18
Shanwang, China	116.5/38.5	1056.2	1107.0	50.7	725.4	1494	768.3	19
Picture Gorge Subgroup, North America	-114.7/44.8	808.9	797.1	-11.8	266	700	434	22
Eastern Oregon, North America	-114/45	808.9	837.1	28.2	266	851	585	23
			MEAN:	245			509	

NOTE: Proxy records from Herold et al. (2010).

^a Where paleo coordinates are not provided by reference values are calculated using modern coordinates, a plate kinematic model and the rotations of Müller et al. (2008).

^b Column three subtracted from column four.

^c Uses the dataset of Willmott and Matsuura (2001) for land precipitation spanning 1950 - 1999.

^d Where a range of values is given, the midpoint is used.

^e Column six subtracted from column seven.

^f References as in Table 2.